

## Electric field gradient study on pure and Cd-doped In(111) surfaces: Correlation between experiments at the atomic scale and first-principles calculations

G. N. Darriba,<sup>1,\*</sup> R. Faccio,<sup>2,†</sup> and M. Rentería<sup>1,‡</sup>

<sup>1</sup>*Departamento de Física and Instituto de Física La Plata (IFLP, CONICET La Plata), Facultad de Ciencias Exactas, Universidad Nacional de La Plata, Casilla de Correo 67, (1900) La Plata, Argentina*

<sup>2</sup>*Centro NanoMat, Cátedra de Física, DETEMA, Facultad de Química, Universidad de la República, Av. General Flores 2124, P.O. Box 1157, Montevideo, Uruguay*



(Received 30 January 2019; revised manuscript received 9 April 2019; published 20 May 2019)

We present a complete all-electron density functional theory/*ab initio* study of structural and electronic properties at pure In(111) and Cd-doped In(111) surfaces, enabling a deep analysis of the electric field gradient (EFG) in these systems. We explained, from first-principles, results of previously performed key time-differential perturbed  $\gamma$ - $\gamma$  angular correlations experiments [W. Körner *et al.*, *Phys. Rev. Lett.* **49**, 1735 (1982)] on <sup>111</sup>In isotopes (which decay to <sup>111</sup>Cd impurity probe-atoms) deposited onto the In(111) surface of thin films under ultrahigh vacuum, adding inactive indium layer by layer, carefully designed to determine the EFG at different depths from the surface. We confirmed the existence of *only* two hyperfine interactions, one related with <sup>111</sup>Cd probes localized at the two more superficial In sites (HFI<sup>S</sup>), and the other related with probes localized in any of the other inequivalent In sites existing from the surface towards the bulk (HFI<sup>B</sup>). In the case of HFI<sup>S</sup>,  $V_{33}$  is oriented normal to the (111) surface, and for HFI<sup>B</sup> we found a  $V_{33}$  orientation parallel to the [001] axis and coincident with the orientation predicted for both the pure and Cd-doped In bulk (not determined experimentally at present), enabling us to confirm the experimental assignment of HFI<sup>B</sup>. The axial symmetry that the EFG has in pure and Cd-doped In bulk systems is broken when the surface is generated and is recovered as the probe (In or Cd, respectively) goes deeper from the surface into the bulk. We separated the structural and electronic effects and their sources in the pure and Cd-doped In(111) surface. For the Cd-doped systems we confirm the experimental ratio  $|V_{33}^S/V_{33}^B| \approx 4$ , showing that light structural modifications have an important impact on the Cd  $p$ -states distribution, which governs the  $V_{33}$  behavior. Finally, from the combination of the predicted  $V_{33}$  for the Cd-doped systems as a function of the depth of the Cd localization from the surface with the experimental fractions of HFI<sup>S</sup> and HFI<sup>B</sup>, we demonstrated that a single 3-Å active monolayer was enough to explain the origin of these fractions (in discrepancy with the previous interpretation of the experiments), proposing a deposition rate for the inactive In layers, in agreement with the experimental fraction evolution as a function of inactive In deposition.

DOI: [10.1103/PhysRevB.99.195435](https://doi.org/10.1103/PhysRevB.99.195435)

### I. INTRODUCTION

In the study of solid systems, hyperfine properties at suitable probe atoms (generally an impurity, but may also be a native atom) provide very valuable physical information (structural, electronic, and magnetic) at the atomic scale. In the case of quadrupole-electric hyperfine interactions, the electric field gradient (EFG) tensor is a quantity that is very sensitive to subtle structural and electronic local variations around a given probe atom. The EFG tensor components are defined by  $V_{ij}(\vec{r}) = \partial^2 V(\vec{r}) / \partial x_i \partial x_j$ ,  $V(\vec{r})$  being the Coulomb potential created by the charge density surrounding the nucleus of the probe atom. Therefore, the rank 2 EFG tensor is symmetric and in the principal axes system it is also traceless due to Poisson's equation, thus being completely defined by only two components: its largest principal component  $V_{33}$

and the asymmetry parameter  $\eta = (V_{11} - V_{22})/V_{33}$ , using the  $|V_{33}| \geq |V_{22}| \geq |V_{11}|$  usual convention.

Time-differential perturbed  $\gamma$ - $\gamma$  angular correlations (TD-PAC) spectroscopy has been intensively employed to investigate structural, electronic, magnetic, and hyperfine properties in a wide variety of compounds and materials (although mainly in bulk) [1–17], since this experimental technique provides a highly precise characterization of the EFG tensor at diluted (ppm) radioactive probe atoms. This probe atom is always the radioactive daughter of a suitable radioactive father isotope adequately introduced (by, e.g., ion implantation) or produced (by chemical methods, neutron activation, etc.) in the host. The  $r^{-3}$  dependence of the EFG from their charge sources makes TDPAC a powerful tool highly sensitive to the anisotropic charge distribution close to the probe nucleus, being able to give very precise information about the local environment of the probe atom. In this experimental spectroscopic technique, the measured quantities are the asymmetry parameter  $\eta$  and the nuclear quadrupole frequency  $\omega_Q$  (proportional to  $V_{33}$ ), given by  $\omega_Q = \frac{\omega_0}{6} = eQV_{33}/4I(2I - 1)\hbar$ . Here  $Q$  is the nuclear quadrupole moment

\*darriba@fisica.unlp.edu.ar

†rfaccio@fq.edu.uy

‡renteria@fisica.unlp.edu.ar

of the sensitive nuclear state (with spin  $I$ ) of the probe atom.

Nowadays, confronting precise experimental determinations of the EFG tensor with very accurate theoretical predictions [9,14,18–26], using all-electron state-of-the-art *ab initio* electronic structure calculations in the framework of the density functional theory (DFT) [27,28], it is possible to obtain valuable information about structural lattice deformations, localization and charge state of impurities and defect centers, impurity energy levels, and structural and magnetic phase transitions, among other interesting properties. The correlation between the EFG and the electronic charge density  $\rho(\vec{r})$  in a physical system is so strong that the agreement between the experimental and predicted EFG validates the  $\rho(\vec{r})$  description and hence all the ground-state properties.

Instead, in thin film solids, there are very few EFG determinations reported in the literature, among which metal systems are the more studied ones. In metallic surfaces, detailed experimental TDPAC studies of the EFG were performed at ( $^{111}\text{In} \rightarrow$ ) $^{111}\text{Cd}$  probes located at different surfaces of indium [29], copper [30–32], silver [33,34], palladium [35,36], and nickel [37,38], showing this technique has great potential to sense surfaces through the study of the EFG tensor, which results in a finger-print of the probe-atom localization and its environment. From all these experimentally studied metallic surfaces, indium is the only metal that has nonzero EFG when a probe atom (native or impurity) is located substitutionally at a defect-free lattice site in bulk conditions. This is a consequence of the symmetry of the In unit cell, that belongs to the tetragonal crystal system, different from the other metals that present cubic crystal systems.

A detailed TDPAC study of the EFG tensor at  $^{111}\text{Cd}$  probes located at and near the In(111) surface was performed by Körner *et al.* [29]. In that work, a sample of 400-Å-thick film of natural indium was evaporated onto a glass backing at 100 K, creating indium substrates with textures, growing preferentially with a (111) surface.  $^{111}\text{In}$  radioactive isotopes, which decay to  $^{111}\text{Cd}$  probes through the electron-capture process, were evaporated (with a typical  $^{111}\text{In}$  concentration of  $10^{-5}$  per inactive In) over the surface at 100 K with a mean thickness of 3 Å. In order to have the probe at different depths from the surface, monolayers of inactive indium were deposited up to 50 Å thick onto the active  $^{111}\text{In}$ -doped indium layer. The authors found, for all depths of the  $^{111}\text{Cd}$  probes, only two hyperfine interactions that we now call  $\text{HFI}^{\text{B}}$  and  $\text{HFI}^{\text{S}}$ .  $\text{HFI}^{\text{B}}$  is characterized by  $|\omega_0^{\text{B}}| = 24(1)$  Mrad/s with a frequency distribution [half width at half maximum (HWHM)] of 15%, axially symmetric (or very close to it) and with  $V_{33}^{\text{B}}$  oriented  $33^\circ$  with respect to the surface plane (i.e., compatible with a  $V_{33}$  orientation parallel to the [001] axis in In bulk), while  $\text{HFI}^{\text{S}}$  is characterized by  $|\omega_0^{\text{S}}| = 102(3)$  Mrad/s with a frequency distribution of 7%, axially symmetric (or very close to it) and with  $V_{33}^{\text{S}}$  oriented perpendicular to the surface, obtaining  $|V_{33}^{\text{S}}/V_{33}^{\text{B}}| \approx 4$ .  $\text{HFI}^{\text{S}}$  and  $\text{HFI}^{\text{B}}$  were associated with the EFG at  $^{111}\text{Cd}$  probes located at the surface and at a great depth from the surface, respectively. With respect to the populations of  $\text{HFI}^{\text{S}}$  and  $\text{HFI}^{\text{B}}$ , 52% of probes sense  $\text{HFI}^{\text{S}}$  and 48% sense  $\text{HFI}^{\text{B}}$  before the inactive indium deposition. For 2 Å of inactive In deposition, 23% of probes sense  $\text{HFI}^{\text{S}}$  and 77% sense  $\text{HFI}^{\text{B}}$ , for 7 Å of inactive In

deposition around 15% of probes sense  $\text{HFI}^{\text{S}}$  and 85% sense  $\text{HFI}^{\text{B}}$ , i.e., the amount of probes that sense  $\text{HFI}^{\text{S}}$  decreases (and therefore the amount of probes that sense  $\text{HFI}^{\text{B}}$  increases) as the probes are located deeper from the surface. In order to explain the ratio  $|V_{33}^{\text{S}}/V_{33}^{\text{B}}| \approx 4$ , the authors performed point-charge-model calculations [39] of the EFG at In atoms in bulk and at the (111) surface of tetragonal In, approximating the complex conduction-electron distribution by point charges centered in the faces of the Wigner-Seitz polyhedra. They studied the EFG on the pure indium system (i.e., not on Cd-doped In), in order to avoid impurity problems (such as unknown structural relaxations and the EFG contribution generated by the Cd electronic shells themselves) and they were only interested in the prediction of this EFG ratio. In addition, for the surface modeling, the atomic reconstruction was not taken into account. In this scenario, they found  $|V_{33}^{\text{S}}/V_{33}^{\text{B}}| \approx 20$ . The high value of the surface's EFG with respect to the bulk value was explained by a modification of the conduction-electron distribution at the surface, and this EFG should be created by the electronic and atomic redistributions as consequence to the symmetry distortion at the surface.

Concerning previous DFT theoretical EFG studies in metallic surfaces, Cottenier *et al.* [40] compared *ab initio* calculations and experimental data results coming from the literature in order to study the coordination dependence of the EFG at Cd impurity sites on fcc (Ni, Cu, Pd, and Ag) metallic surfaces, studying the terrace and the adatom sites for each surface. It is worth mentioning that, in opposition to the experimental nonzero EFG in bulk tetragonal indium, the bulk EFGs in the FCC systems studied in Ref. [40] are null, showing the potential differences in the structural properties between both types of reconstructed surfaces.

Here, we present a complete and detailed theoretical *ab initio* study of isolated Cd impurities located at and near the In(111) surface, at substitutional In sites as a function of the depth of the impurity with respect to the surface. Nevertheless, before we introduce completely the study of the Cd-doped In(111) surface, we study, as a first step, the reconstruction of the undoped (pure) In(111) surface, in order to be able to use this reconstructed surface of the pure system as a starting point in the study of a Cd-doped In(111) surface. In addition, we performed *ab initio* calculations for pure and Cd-doped In bulk (tetragonal) systems, with the aim of characterizing the effects on the EFG introduced by both the new boundary condition (surface generation and reconstruction) and the inclusion of the impurity itself. Finally, confronting all the above mentioned *ab initio* predictions with the existing EFG experimental results for the  $^{111}\text{Cd}$ -doped In(111) surface [29] and at the pure [41–46] and  $^{111}\text{Cd}$ -doped indium bulk site [37,41,47], we explained the origin of the EFG at and near the (111) surface of pure and Cd-doped In. From this comprehensive study we could explain the hyperfine interactions observed at  $^{111}\text{Cd}$  atoms deposited onto the In(111) surface of thin films grown layer by layer, proposing a deposition model that explains the presence of the bulk interaction already when the active monolayer does not have any additional inactive layer deposited on it.

In this way, the understanding of the origin and behavior of the hyperfine properties at the reconstructed  $^{111}\text{Cd}$ -doped

surfaces allows us to demonstrate the importance of this extremely local and sensitive physical magnitude to evaluate electronic and structural properties in the proximity of surfaces.

This paper is organized as follows. In Sec. II we describe the methodology employed in the calculations, describing the surface simulation procedure and the utilized theoretical approach. In Sec. III we present the theoretical results for the structural properties and the EFG predictions as a function of the probe's depth from the surface, for an undoped and Cd-doped In(111) surface and in bulk, and their comparison with experimental results coming from the literature, interpreting the EFG behavior. In Sec. IV we discuss and reinterpret the experimental results on a  $^{111}\text{Cd}$ -doped In(111) surface, explaining the origin of the hyperfine interactions observed and proposing a different deposition model. Finally, in Sec. V we present our conclusions.

## II. METHODOLOGY

For the In(111) surface generation we started from the bulk In tetragonal unit cell, which belongs to the  $I4/mmm$  space group, with  $a = b = 3.2520(2) \text{ \AA}$  and  $c = 4.9466(2) \text{ \AA}$  [48]. In Fig. 1(a) we show the (111) plane of the In bulk supercell (SC) in its tetragonal representation, and in Fig. 1(b) we show the set of  $a'$ ,  $b'$ , and  $c'$  unit cell parameters that will be used to simulate the In(111) surface. That surface was modeled employing the  $a'b'c'$  representation, using the SC method together with the slab approximation, i.e., cutting the SC at a plane parallel to the  $b'-c'$  plane and introducing a vacuum space along the  $a'$  axis, as shown in Fig. 1(c) (note that the  $a'$  direction and the vector normal to the  $b'-c'$  plane are at about  $23^\circ$ ). With this kind of cut, there is a unique termination to form the In(111) surface. We must clarify that although in the  $a'b'c'$  representation the cutting plane is now the (100), we will continue to call the generated surface as (111), independently of the axis system used in the representation. In our study, we probe that the vacuum region between adjacent slabs greater than  $12 \text{ \AA}$  is sufficient to neglect electronic interaction between periodic images, both for pure and Cd-doped In(111) surfaces.

For pure In systems, the (111) surfaces were simulated using a  $14a' \times 1b' \times 1c'$  ( $14 \times 1 \times 1$ ) SC, where four of these 14 unit cells in the  $a'$  direction were used to simulate the vacuum and the other ten unit cells were used to simulate the slab. With this geometry we have five unit cells in the  $a'$  direction to obtain inequivalent In atoms from the surface to a depth of about  $16 \text{ \AA}$ . The depth of the In atom from the surface is measured along the  $Z$  direction, normal to the (111) plane, which is not parallel to the [111] direction (i.e., the  $a'$  axis). This system, without any relaxation of the atomic positions, is called the *just generated surface*. In this system, forces at In atoms appear, which are much stronger as the In atom approaches the surface. For this reason, we performed a complete relaxation of the atomic positions of all atoms in the just generated SC, in order to find the *reconstructed surface*, i.e., the equilibrium structure of this surface. From here on we establish the  $\text{In}_i$  ( $i = 1-16$ ) notation, with the  $i$  subscript increasing as the In atom moves away from the surface into

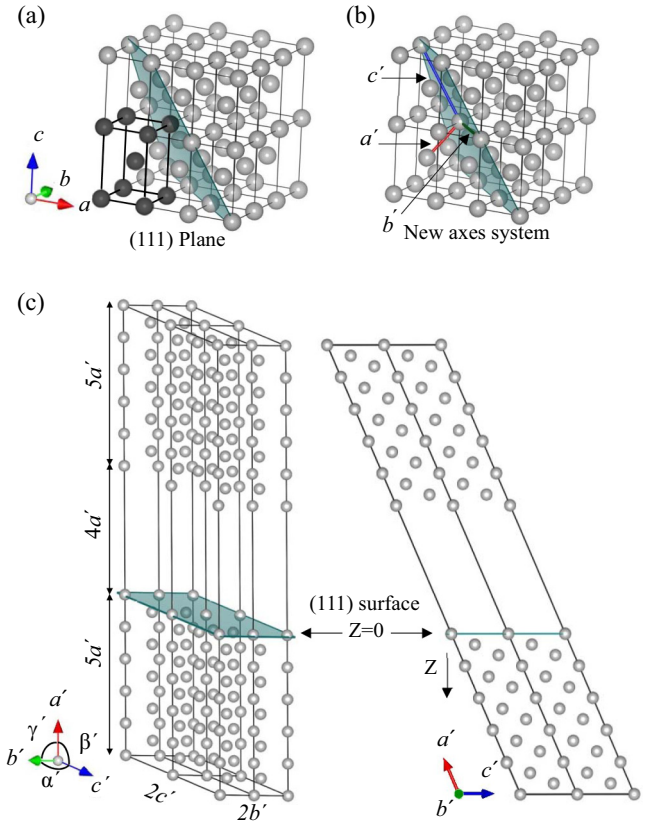


FIG. 1. (a) Indium structure in its tetragonal representation showing the (111) plane (unit cell in dark color), (b) Our  $a'b'c'$  axes system used to generate the surface, and (c)  $14 \times 2 \times 2$  supercell used to generate the In(111) surface. The  $Z$  direction, which measures the depth of the In atoms from the surface, is normal to the (111) plane and is not parallel to the [111] direction ( $a'$  axis). The plane corresponds to  $Z = 0 \text{ \AA}$  (plane containing the topmost In atom in the surface).

the bulk; therefore  $\text{In}_1$  is the topmost In atom in the surface and  $\text{In}_{16}$  is the deepest one.

In order to simulate an isolated impurity, we replaced an In atom by a Cd one in the SC used to simulate the pure In(111) surface, but duplicating the size of the SC in the  $b'$  and  $c'$  directions ( $14 \times 2 \times 2$  SC). We duplicated the size of the SC along the  $b'$  and  $c'$  directions [with respect to those used for the pure In(111) surfaces] with the aim to eliminate the undesired Cd-Cd interactions, and to be closer to the conditions of diluted probe atoms used in hyperfine experimental techniques. The Cd atom was located at the different In sites in order to obtain In surfaces with the Cd impurity atom located at different depths from the surface. It should be clarified that each studied doped surface has a unique Cd impurity atom located at a given depth from the surface. From here on we establish the  $\text{In} : \text{Cd}_i$  ( $i = 1-16$ ) notation for the Cd-doped systems in the In(111) surfaces, with the  $i$  subscript increasing as the Cd impurity moves away from the surface into the bulk; e.g., in  $\text{In} : \text{Cd}_1$  the Cd atom replaces the topmost In atom (i.e., replacing the  $\text{In}_1$  atom).

All-electron electronic structure *ab initio* calculations within the DFT formalism [27,28] were performed in order to determine the equilibrium atomic positions of each studied system and, from the accurate description of the electronic density  $\rho(\vec{r})$ , the EFG tensor. The calculations were performed using the VASP code (Vienna *Ab Initio* Simulation Package) [49–53]. The projector augmented wave (PAW) method [53,54] was employed to account for the electron–ion core interaction, utilizing the generalized gradient approximation (GGA) exchange–correlation functional with the Perdew–Burke–Ernzerhof (PBE) parametrization [55]. We used the PAW-PBE potentials with the following valence electrons: In ( $5s^2 5p^1$ ) and Cd ( $4d^{10} 5s^2$ ). The  $k$ -space grid of  $1 \times 6 \times 6$  and a cutoff energy for the plane wave expansion of 300 eV were selected in all the calculations. The structures were relaxed until the forces in all the atoms were lower than 0.01 eV/Å, and the unit cell was optimized until the components of the stress tensor were lower than 1 kbar. The unit cell parameters were optimized only for pure In bulk and then were kept fixed for the study of all the surface systems, in which the atomic forces were minimized to obtain the final equilibrium atomic positions. In addition, to compare the EFG predictions in the undoped In(111) surface; In:Cd<sub>1</sub>, In:Cd<sub>2</sub>, and In:Cd<sub>16</sub> surface systems; and for undoped and Cd-doped In bulk, we performed calculations using the full-potential augmented plane wave plus local orbital (FP – APW + lo) method [56], employing the WIEN2K code [57], in order to compare the predicted results of both different *ab initio*/DFT methods. In the cases of the surface systems we started the FP – APW + lo relaxation refinement from the equilibrium atomic positions predicted by VASP in each case (i.e., in the pure and Cd-doped surfaces), which is a much faster way to obtain the atomic equilibrium positions in surface systems. The FP – APW + lo calculations were performed using the PBE-GGA parametrization for the exchange–correlation functional and the same  $1 \times 6 \times 6$   $k$ -space grid used in the VASP simulations. The cutoff parameter of the plane wave bases in the interstitial region was  $R_{\text{MT}}K_{\text{max}} = 7$ , where  $K_{\text{max}}$  is the maximum modulus of the lattice vectors in the reciprocal space, and  $R_{\text{MT}}$  is the smallest radius of the nonoverlapping muffin-tin spheres centered in the atoms. In our calculations we use for Cd and In  $R_{\text{MT}} = 1.06$  Å.

It is well known that the FP – APW + lo method describes very accurately the electronic charge density in a crystalline system, providing in this way a correct prediction of the EFG tensor that depends strongly on the anisotropy of this density in the close neighborhood of the atomic nucleus. We performed *ab initio* calculations with both methods in order to check the electronic density, and therefore the EFG, predicted by the VASP code. We will show that the results obtained with both *ab initio* methods, in the key systems in which the comparison was done, are closely the same, predicting the same electronic and equilibrium structures, and therefore the same EFG tensor. In this way, since the VASP code requires less computing capability than WIEN2K, the systematic calculation in the doped surfaces can be performed and discussed with the VASP code. It should be mentioned that the check of the VASP accuracy in predicting the EFG is not trivial; for this reason we checked both the pure and doped systems. Finally, spin-orbit coupling was neglected in all the

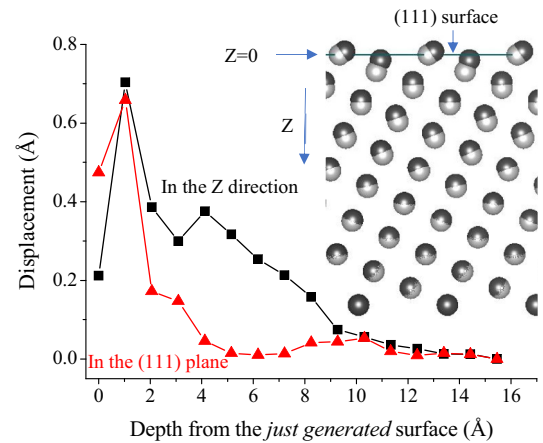


FIG. 2. Displacement of the In atoms in the reconstructed In(111) surface with respect to their positions in the just generated surface, along the  $Z$  direction (black squares) and in the (111) plane (red triangles), as a function of the depth from the just generated surface. The relative positions of the atoms of the reconstructed (dark gray spheres) and just generated (light gray spheres) In(111) surface in a plane normal to this surface are sketched on the right.

calculations, since selected tests indicated that the changes in the hyperfine parameters vary less than 5%, thus not affecting any trend nor the conclusions.

### III. RESULTS

#### A. Undoped In(111) surface

In this section we study the reconstruction of the undoped In(111) surface, structural starting point of the Cd-doped In(111) surfaces, to separate the effects introduced by the Cd impurity and those by the surface boundary conditions. Also, to understand the unexpected EFG behavior near the edge of the undoped reconstructed surface, we need to describe the structural and electronic modifications generated by the free relaxation on the just generated surface.

In Fig. 2 we compare the position of the In atoms in the just generated In(111) surface (light gray spheres) and in the reconstructed surface, i.e., when the atoms reach their final equilibrium positions (dark gray spheres). As we see, the displacement of the In atoms is stronger as the In atom approaches the surface, either along the direction normal to the (111) surface ( $Z$  direction in Fig. 2) or in the (111) plane. In effect, the In atom that is located immediately below the surface (In<sub>2</sub>) experiences the greatest displacement when the surface is freely relaxed. The displacement of all In atoms in the direction normal to the (111) surface is always towards the surface.

Due to the boundary surface conditions, the topmost In atom (In<sub>1</sub>) has only six nearest neighbor atoms (NN = 6), and the In<sub>2</sub> and In<sub>3</sub> atoms, which are located just below the In<sub>1</sub>, have NN = 9 and NN = 11, respectively. The rest of the In<sub>*i*</sub> atoms in the SC (from In<sub>4</sub> to In<sub>16</sub>) have NN = 12, as in the bulk, four of these neighbors being at the same distance and the other eight at a distance slightly larger than the previous one. When the In(111) surface reaches its equilibrium structure, the system relaxes and the NN distances ( $d_{\text{NN}}$ ) for

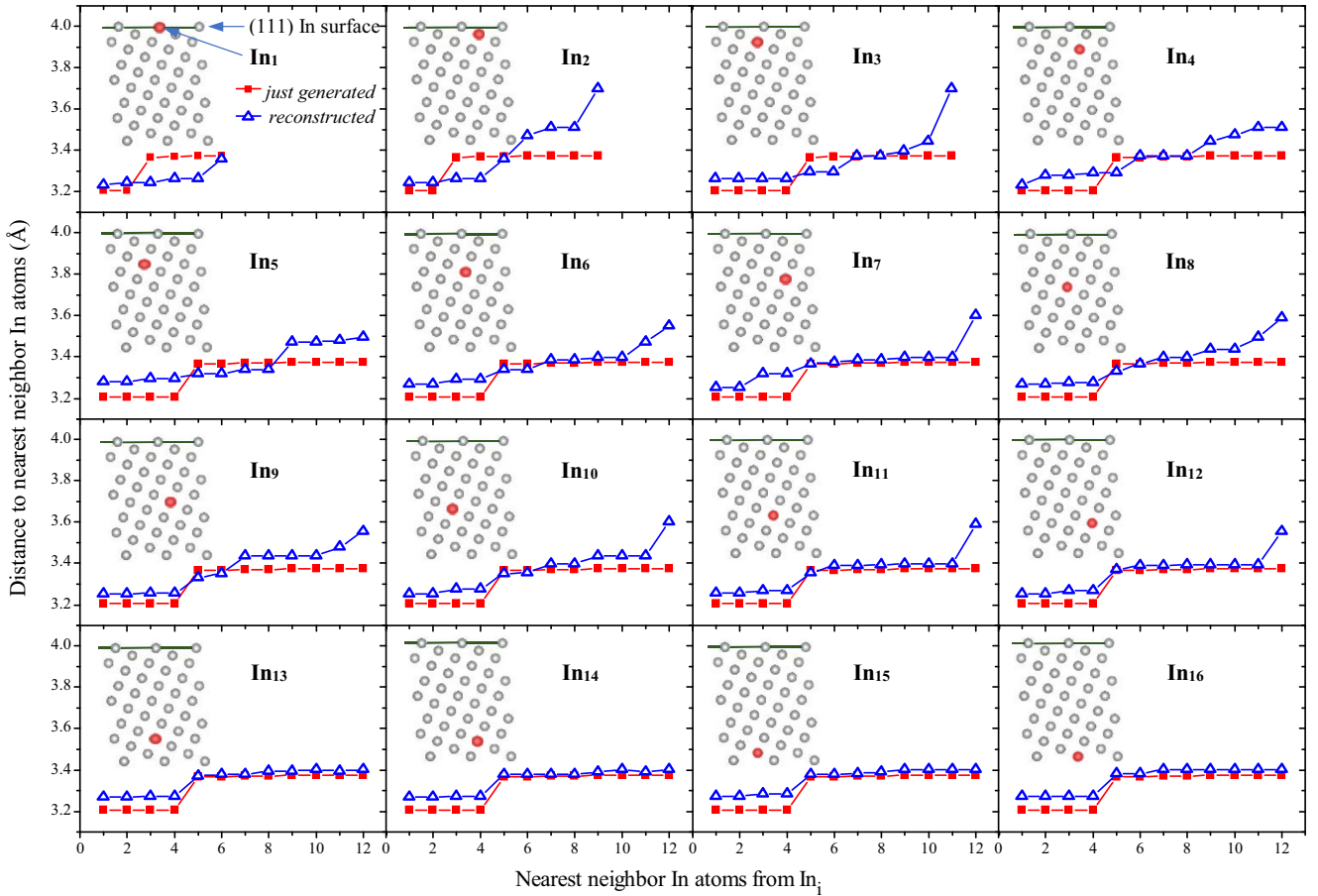


FIG. 3. Increasing distances from each inequivalent  $\text{In}_i$  ( $i = 1$  to 16) atom to its nearest neighbor In atoms ( $d_{\text{NN}}$ ) into the SC ( $\text{In}_i$  is indicated as a red atom in the schematic slab shown in each panel). The red squares correspond to the just generated surface and the blue open triangles to the reconstructed surface. The horizontal axis only shows a numeration of the nearest neighbor In atoms. The label does not indicate necessarily the same atom for the just generated and reconstructed systems; the numeration is just chosen to present a monotonous trend.

the inequivalent In atoms change. In Fig. 3, we plot  $d_{\text{NN}}$  for each inequivalent  $\text{In}_i$  atom into the SC, for the just generated surface (squares) and those corresponding to the reconstructed surface (triangles).

As we see in Fig. 3,  $d_{\text{NN}}$  for  $\text{In}_1$  and  $\text{In}_2$  are the ones that suffer the greatest changes. As we move away from the surface,  $d_{\text{NN}}$  in the relaxed system tend to those they have in the nonrelaxed one (the triangles tend to overlap the squares), showing that the structural distortions introduced by the surface disappear as we move away from the discontinuity generated to simulate this surface. In effect, as the In atom moves away from the surface it has an environment similar to what it has in the bulk system. In addition, when we relax the equilibrium structure predicted by VASP with the WIEN2K code, we found variations less than  $10^{-3}$  Å in  $d_{\text{NN}}$ , predicting the same reconstructed surface.

Let us now present the predicted results for the EFG tensor at each inequivalent In site. In Fig. 4 we present the predicted values for  $V_{33}$  (the largest EFG component), in the just generated In(111) surface, i.e., without relaxation of the atomic positions. As we can see, the predicted  $V_{33}$  values by VASP and WIEN2K are almost the same, very little difference existing for the two most superficial In atoms, that are within the convergence error of the simulations. The same agreement

between VASP and WIEN2K predictions was found for  $V_{11}$  and  $V_{22}$ , not shown for clarity in Fig. 4. Comparing these  $V_{33}$

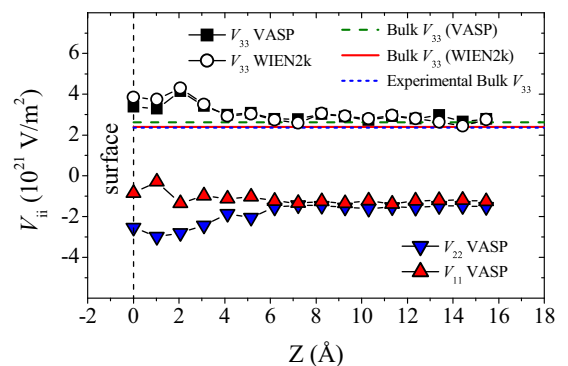


FIG. 4. Predicted EFG components as a function of the depth of the In atom from the just generated In(111) surface. The dashed (green) and dotted (blue) lines represent the  $V_{33}$  predictions for the In bulk system by VASP and WIEN2K, respectively. The solid (red) line represents the  $|V_{33}|$  value determined experimentally at In bulk by different nuclear techniques and different In isotopes [41–46].  $Z = 0$  Å is the position of the topmost In atom in the just generated pure In(111) surface.

values with those coming from our bulk predictions and the experimental values determined in bulk systems (discussed later), it is evident that there are not very relevant effects in the  $V_{33}$  behavior when the surface is generated. In effect, the surface generation produces an increase in the value of  $V_{33}$  of only 30%–50% at the more superficial ( $Z \leq 2 \text{ \AA}$ ) In atoms. Inspecting the  $V_{11}$  and  $V_{22}$  behavior we can see that the EFG loses symmetry as the probe approaches the surface. For In atoms deeper than  $6 \text{ \AA}$ ,  $V_{11}$  and  $V_{22}$  tend to the same value, indicating that the EFG tensor recovers the axial symmetry ( $\eta \rightarrow 0$ ) that it has in In bulk [41], and therefore the complete EFG tensor converges to that of the bulk structure.

In Fig. 5, we present the behavior of the EFG tensor in the reconstructed In(111) surface (i.e., once the equilibrium atomic positions of all atoms of the system are achieved) as a function of the depth of the In atom from the surface. Just like on the just generated In(111) surface, the EFG tensors predicted by VASP and WIEN2K are very similar, showing for clarity in this figure only the WIEN2K predictions for  $V_{33}$ . In this way we proved that for the same atomic positions both methods predict the same electronic density in the pure system. On the other hand, the result of the equilibrium structures after the structural relaxations are basically the same, predicting the same EFG with both methods.

Comparing Figs. 4 and 5(a), we can see that although the  $V_{ii}$  values for the most superficial In atoms change (even in sign), the values of the EFG components (i.e.,  $V_{11}$ ,  $V_{22}$ , and  $V_{33}$ ) are converged when the In atom are located deeper than  $5 \text{ \AA}$  from the surface. As it happens in the just generated surface,  $V_{11}$  and  $V_{22}$  tend to the same value, indicating that the EFG tensor recovers the axial symmetry ( $\eta \rightarrow 0$ ) that it has in In bulk [42]. This recovery of the bulk values for atoms located deeper than  $5$  or  $6 \text{ \AA}$  from the surface, in pure systems, was already found in the *ab initio* study of a pure  $\alpha\text{-Al}_2\text{O}_3(001)$  surface [58].

In Fig. 5(b) we show the predictions of  $|V_{33}|$  and again its comparison with values predicted by us and the experimental ones obtained for indium bulk systems. It should be noted that we show  $|V_{33}|$  because it is the usual magnitude determined experimentally. The apparent change in  $V_{33}$  sign at In<sub>3</sub> and In<sub>4</sub> is not a real physical change in the behavior of  $V_{33}$  along the  $Z$  direction. Due to the high asymmetry parameter at these sites [see that  $|V_{22}|$  is almost similar to  $|V_{33}|$  in Fig 5(a)],  $V_{33}$  or  $V_{22}$  can be interchanged since the largest EFG principal component can be either  $V_{33}$  or  $V_{22}$  upon subtle variations in the electronic density, conserving the  $V_{33}$  and  $V_{22}$  monotonous trend as in the just generated surface. Comparing  $V_{33}$  in Fig. 4 and  $|V_{33}|$  in Fig. 5(b) we show that the full structural relaxation does not introduce any relevant change in the EFG behavior, except at the In<sub>2</sub> position which will be discussed below. In Fig. 5(b), the dashed (green) and dotted (blue) lines indicate the predicted  $V_{33}$  values in the bulk indium system by VASP ( $V_{33} = 2.62 \times 10^{21} \text{ V/m}^2$  in the [001] direction and  $\eta = 0$ ), and WIEN2K ( $V_{33} = 2.36 \times 10^{21} \text{ V/m}^2$  in the [001] direction and  $\eta = 0$ ), respectively, while the red solid line indicates the experimental  $V_{33}$  value reported in the literature by different techniques at  $T = 4.2 \text{ K}$ . The experimental value of the quadrupole frequency  $\nu_Q$  comes from experiments of nuclear quadrupole alignment (NQA) using  $^{114}\text{In}$  as probe [43], nuclear quadrupole resonance (NQR) using  $^{115}\text{In}$  as

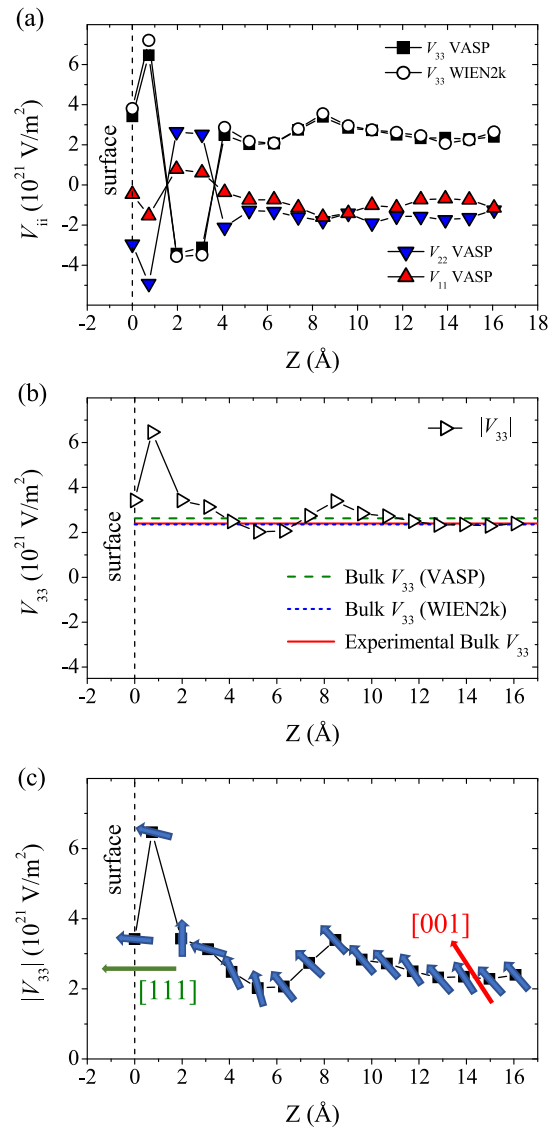


FIG. 5. (a) Predicted EFG components as a function of the depth of the In atom from the reconstructed In(111) surface. (b) Comparison of predicted  $|V_{33}|$  (white triangles) as a function of the depth of the In atom from the surface with experimental and our predicted values of  $V_{33}$  in In bulk. The red line represents the  $|V_{33}|$  value determined experimentally in In bulk by different nuclear techniques and different In isotopes [41–46]. (c) Predicted  $V_{33}$  direction at the In site as a function of its depth from the In(111) surface. The red and green arrows show the crystalline [001] direction and a direction normal to the (111) surface, respectively.  $Z = 0 \text{ \AA}$  is the position of the topmost In atom in the reconstructed pure In(111) surface.

probe [42,44–46], and TDPAC using  $^{117}\text{In}$  as probe [41]. The experimental EFG is axially symmetric [41] and using the nuclear quadrupole moments  $Q$  of  $^{114}\text{In}$ ,  $^{115}\text{In}$ , and  $^{117}\text{In}$  determined by Errico and Rentería [59], we have, using the relationship  $\nu_Q = eQV_{33}/h$ , where  $e$  is the electron charge,  $h$  the Planck constant,  $V_{33} = 2.4 \times 10^{21} \text{ V/m}^2$  for all experimental measurements mentioned above. In all these experiments, the  $V_{33}$  orientation was not determined. In Fig. 5(b) the red line includes the errors in the  $V_{33}$  determination taking into account

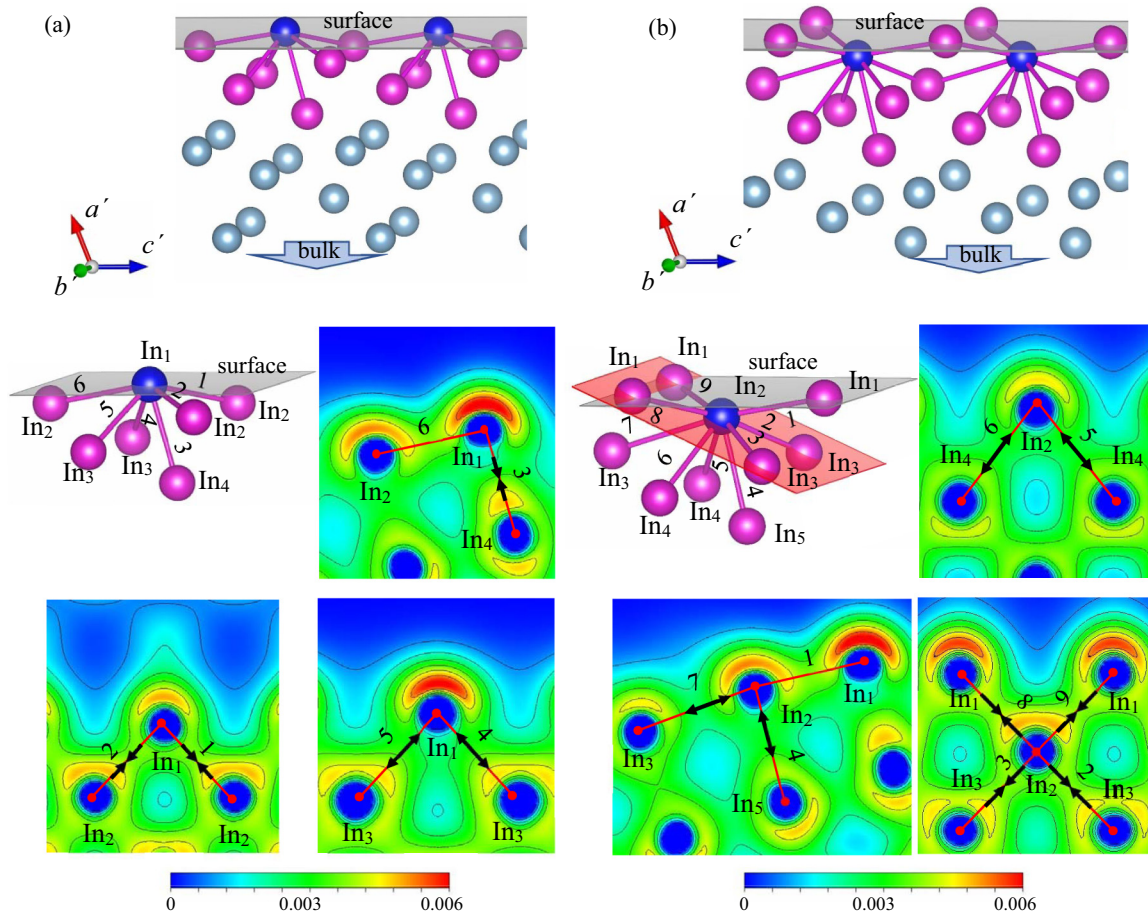


FIG. 6. (a)  $\text{In}_1$  (in blue) and (b)  $\text{In}_2$  (in blue) nearest neighbors coordination (the rest of the  $\text{In}_i$  atoms are in magenta) of the reconstructed  $\text{In}(111)$  surface (middle-left panels). The  $\text{In}_1$ - $\text{In}_i$  and  $\text{In}_2$ - $\text{In}_i$  bonds are arbitrarily labeled. The  $\text{In}_1$  (or  $\text{In}_2$ ) site and the indicated bonds determine the different planes in which the electronic density plots  $\rho_{cc}(\vec{r})$  (see text) are shown. In these plots, the arrows indicate the direction of the relaxation along the indicated bond. The atomic positions and bonds are in red in the  $\rho_{cc}(\vec{r})$  plots. The top panels in (a) [(b)] show the  $\text{In}_1$ - $\text{In}_1$  ( $\text{In}_2$ - $\text{In}_2$ ) coordination and localization with respect to the surface and the other deeper  $\text{In}$  atoms (in light blue).

the propagated error in the  $Q$  determination of the  $\text{In}$  isotopes. In summary, Fig. 5(b) shows that for  $\text{In}$  atoms located deeper than 5 Å from the (111) surface, the converged values of  $V_{33}$  are in excellent agreement with the  $V_{33}$  value measured and predicted in the bulk system. Nevertheless, taking into account the discussion about the interchange between  $V_{33}$  and  $V_{22}$ ,  $V_{33}$  recovers its bulk value immediately below the surface [see the triangles in Fig. 5(b) for  $\text{In}_3$ ]. It is worth noting that the ratio of  $V_{33}$  at  $\text{In}$  atoms localized at the surface sites (except  $\text{In}_2$ ) and at the bulk in  $\text{In}$  systems (around 1.5 times) is very small compared with the ratio  $|V_{33}^S/V_{33}^B| \approx 4$  found for pure  $\alpha$ - $\text{Al}_2\text{O}_3$  surface [58].

Finally, with respect to the  $V_{33}$  direction, we can see in Fig. 5(c) that it is perpendicular to the (111) surface for the two more superficial  $\text{In}$  atoms. For  $\text{In}$  atoms located deeper than 4 Å from the (111) surface, the  $V_{33}$  direction converges to the [001] direction (of the tetragonal  $\text{In}$  unit cell), which is coincident with the predicted  $V_{33}$  orientation in  $\text{In}$  bulk. In view of the lack of experimental determination of this observable, our prediction gives accurate knowledge of it. Finally, inspecting the complete Fig. 5, we see that the EFG tensor recovers its bulk value (magnitude, symmetry, and direction) for  $\text{In}$  atoms located deeper than 5 Å.

We will discuss in more detail the unexpected behavior of the EFG near the surface (at  $\text{In}_1$  and  $\text{In}_2$  sites) before and after the surface reconstruction, trying to understand the origin of this effect. The question that arises is why  $V_{33}$  does increase a lot at the  $\text{In}_2$  site after the reconstruction, while at the  $\text{In}_1$  site  $V_{33}$  remains almost constant (see Figs. 4 and 5). Figure 6 shows the nearest neighbors coordination of  $\text{In}_1$  and  $\text{In}_2$  in the reconstructed  $\text{In}(111)$  surface, with the  $\text{In}_1$ - $\text{In}_i$  and  $\text{In}_2$ - $\text{In}_i$  arbitrarily labeled. This figure also shows electronic density plots [called herein  $\rho_{cc}(\vec{r})$ ] for selected planes containing  $\text{In}_1$  or  $\text{In}_2$  atoms and different  $\text{In}_1$ - $\text{In}_i$  or  $\text{In}_2$ - $\text{In}_i$  bonds, filtered from an energy range of 1 eV below the Fermi level (“conduction electrons”). The arrows indicate the direction of the bond-length relaxation after the reconstruction process for each bond. In the case of the  $\text{In}_2$  site, the only four NN atoms that considerably share electron charge with the  $\text{In}_2$  atom are localized in a same plane (plotted in red) and move towards it, while the four NN atoms that do not share charge with the  $\text{In}_2$  atom move away from it. The bond (bond 1) that presents the highest electron density does not change its bond length. The EFG at the  $\text{In}_2$  site is generated by the nonspherical electron density close to the  $\text{In}_2$  nucleus. Hence the EFG will change only if this electron density changes, as

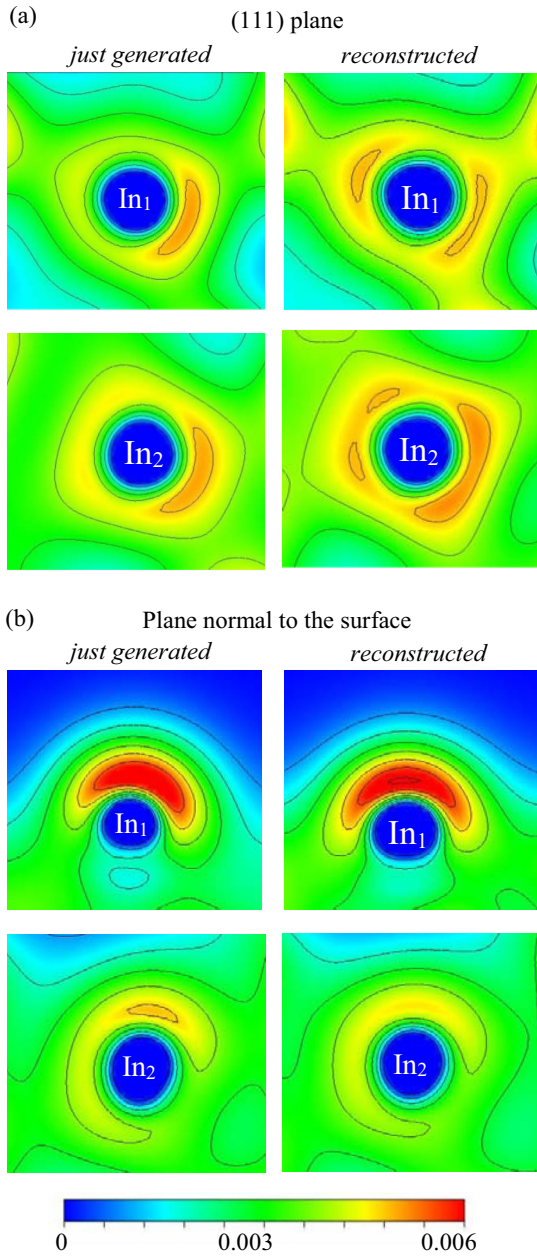


FIG. 7. Electronic density plots  $\rho_{ce}(\vec{r})$  (see text) at  $\text{In}_1$  and  $\text{In}_2$  before (left column) and after (right column) the (111) surface reconstruction for (a) a plane parallel to the (111) surface and (b) a plane containing  $V_{33}$ , i.e., normal to the (111) surface.

is apparent for the  $\text{In}_2$  site. In turn, the EFG at the  $\text{In}_1$  site does not change upon reconstruction. This can be understood noting that the bond length (bond 6) with the highest density does not change, the bond length (bond 3) which is shortened does not share charge between  $\text{In}_1$  and  $\text{In}_4$ , and the bonds that share charge between  $\text{In}_1$  and  $\text{In}_2$  (bonds 1 and 2) or  $\text{In}_3$  (bonds 4 and 5) are shortened and enlarged, respectively, compensating the effect.

In order to analyze the effect of the charge modification on  $V_{33}$  at both  $\text{In}_1$  and  $\text{In}_2$  atoms, we plot in Fig. 7  $\rho_{ce}(\vec{r})$  at  $\text{In}_1$  and  $\text{In}_2$  in selected planes, one normal to the  $V_{33}$  direction [Fig. 7(a)] and another that contains  $V_{33}$  [Fig. 7(b)], before

and after the surface reconstruction (left and right columns, respectively). Once the principal axis system is known, negative electronic charge localized in the  $V_{11}$ - $V_{22}$  plane (plane normal to  $V_{33}$ ) contributes positively to  $V_{33}$ , while negative charge localized along the  $V_{33}$  axis generates a negative contribution to  $V_{33}$ . In this sense, the density plots at  $\text{In}_2$  in Fig. 7 show an accumulation of electron charge in the  $V_{11}$ - $V_{22}$  plane and depletion of charge along the  $V_{33}$  axis, hence showing an increase of  $V_{33}$  at  $\text{In}_2$ . On the other hand, there is a little charge accumulation in the  $V_{11}$ - $V_{22}$  plane at  $\text{In}_1$  and also along the  $V_{33}$ , suggesting a compensating effect upon  $V_{33}$ .

To confirm the precedent simple and graphical analysis, we studied the EFG behavior using the so-called asymmetry count of the electronic charge. In our studied system, the completely filled  $d$  shell of the In atoms does not contribute to the EFG. Therefore, it is enough to analyze only the EFG contribution of the  $p$  electrons. In this case the value of  $V_{33}$  is proportional to the  $p$  electrons asymmetry count, defined as  $\Delta n_p = \frac{1}{2}(n_{p_1} + n_{p_2}) - n_{p_3}$ , where  $n_{p_i}$  is the number of electrons in the  $p_i$  orbital, along the direction of  $V_{ii}$ . Numerical evaluation of  $n_{p_i}$  at the  $\text{In}_2$  site, before and after the reconstruction of the undoped In(111) surface, shows a strong increase in  $\Delta n_p$ , explaining the increase in  $V_{33}$  after the surface reconstruction. On the other hand,  $\Delta n_p$  (and hence  $V_{33}$ ) for  $\text{In}_1$  and  $\text{In}_2$  are basically the same in the just generated surface, but when we reconstruct the surface achieving its equilibrium structure,  $\Delta n_p(\text{In}_1)$  remains constant and  $\Delta n_p(\text{In}_2)/\Delta n_p(\text{In}_1) \approx 1.8$ , reflecting the great increment of  $V_{33}$  at the  $\text{In}_2$  position.

The fact that the asymmetry parameter is not equal to zero at the two most superficial In sites ( $\text{In}_1$  and  $\text{In}_2$ ) indicates that the charge accumulation at these sites in the surface plane is not symmetrically distributed [i.e.,  $n_{p_1}$  and  $n_{p_2}$  differ, as seen in Fig. 7(a) on the right].

## B. Cd-doped In(111) surface

After the study of the reconstruction of the undoped (111) surface, we present the results for isolated Cd impurities located at substitutional In sites in this surface, as a function of the Cd's depth from the surface. We started the reconstruction of the different Cd-doped systems [the In (111) surface with Cd atoms at different depths] from the reconstructed undoped In surface since our aim was to try to separate the effects generated by the presence of the surface and those generated by the presence of the Cd impurity (electronic effects). With all this information, we want to identify, characterize, and understand the structural, electronic, and hyperfine properties introduced by the Cd impurity in the framework of this boundary condition.

As in the In bulk system, the presence of a Cd impurity replacing a native In atom introduces forces at the Cd atom and the rest of the In atoms in the SC, being these forces extremely strong at the nearest In neighbors. For this reason, we performed a full relaxation of all atoms, starting from the reconstructed undoped (111) surface with one Cd atom located at a given depth from the surface, in order to obtain the equilibrium structure for each system. When Cd is localized at the topmost In site ("In:Cd<sub>1</sub> system"), it sinks 0.235 Å with respect to the reconstructed surface formed by the rest of

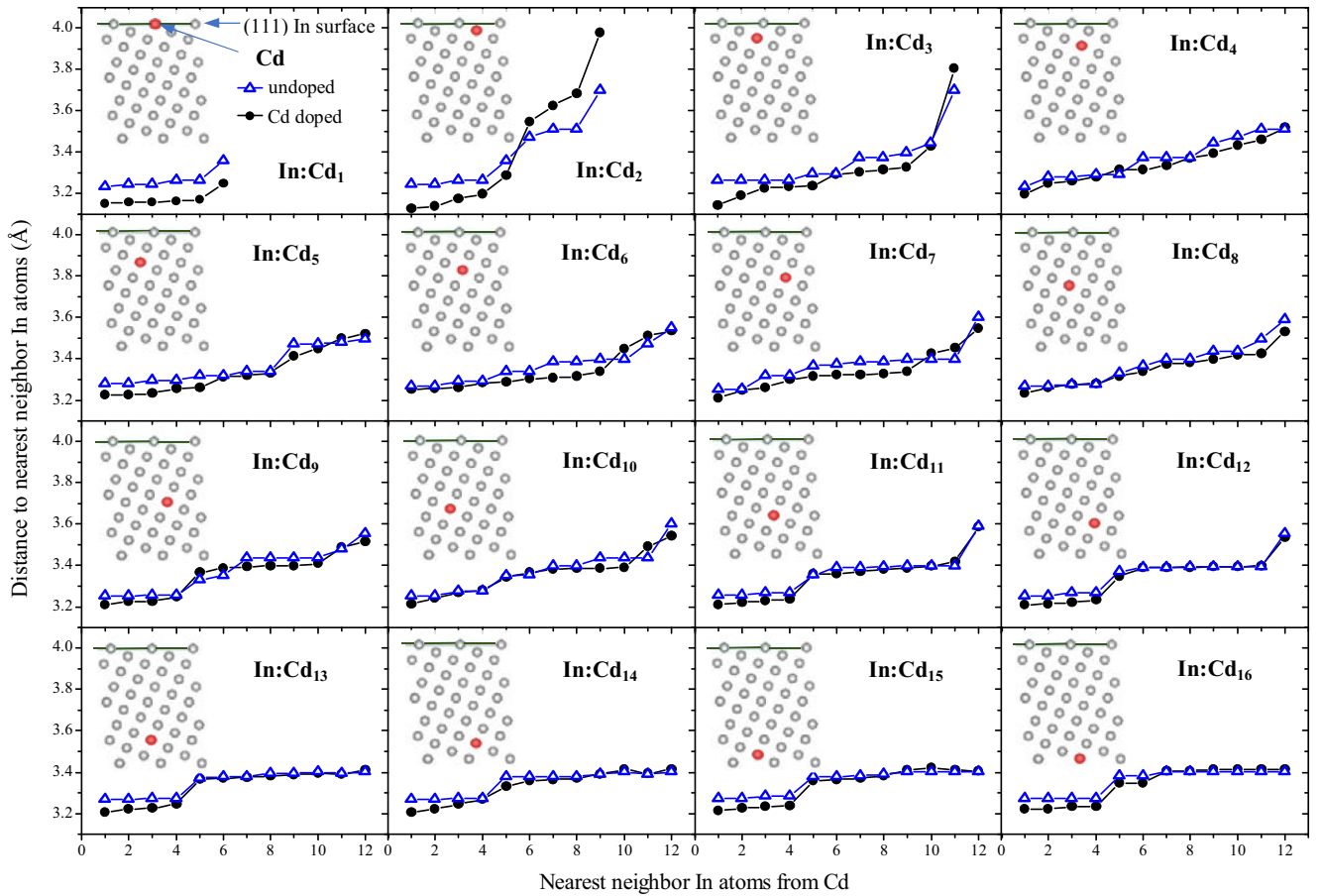


FIG. 8. Distances from each inequivalent Cd atom to its nearest neighbor In atoms for the In : Cd<sub>*i*</sub> (*i* = 1–16) systems (Cd is indicated as a red atom in the schematic slab shown in each panel). The blue open triangles correspond to the undoped reconstructed In(111) surface and the black circles to the Cd-doped reconstructed In(111) surface. The horizontal axis only shows a numeration of the Cd's nearest neighbor In atoms. The label does not indicate necessarily the same atom for the undoped and Cd-doped systems. This numeration has simply been chosen to show a monotonous trend.

the topmost In<sub>1</sub> atoms. On the other hand, the reconstruction of the surface terrace, as the Cd impurity is located deeper from the surface towards the bulk, tends to the reconstructed undoped In(111) surface, showing that the effects produced by the Cd impurity in the surface termination are negligible as the Cd atom moves away from it.

When each Cd-doped In(111) surface (In : Cd<sub>*i*</sub> system) reaches its equilibrium structure, the Cd-In<sub>NN</sub> distances ( $d_{NN}$ ) change with respect to the In<sub>*i*</sub>-In<sub>NN</sub> distances in the undoped reconstructed In(111) surface, as shown in Fig. 8. As can be seen, the  $d_{NN}$  have greater changes as the Cd atom approaches the surface, and practically do not change for the deeper Cd atoms. However, even for the deepest Cd atom, the four nearest In neighbors are at shorter distances than those they have around the native In<sub>16</sub> of the reconstructed (111) surface. This behavior is in agreement with the fact that when a Cd impurity replaces a native In atom in bulk, and this system reaches its equilibrium structure,  $d_{NN}$  experience a small isotropic contraction. For the key In:Cd<sub>1</sub>, In:Cd<sub>2</sub>, and In:Cd<sub>16</sub> systems, i.e., near the (111) surface and at the deepest Cd site, we performed an additional relaxation employing the WIEN2K code, starting from the equilibrium structure predicted by VASP in each system. We found differences in  $d_{NN}$  less than 1.4%,

0.5%, and 0.3% for In:Cd<sub>1</sub>, In:Cd<sub>2</sub>, and In:Cd<sub>16</sub>, respectively, showing that both methods predict, basically, the same equilibrium structures for the Cd-doped systems. The refinement in the atomic positions performed with the WIEN2K code is not relevant from the structural point of view in the Cd-doped surface, as we also showed in the previous section for the pure In(111) surface. Moreover, as occurred in the pure surface, the EFG results at the key Cd positions of the Cd-doped surface are almost equal to those predicted by VASP [see Fig. 9(b)], enabling us to analyze with VASP the EFG behavior as a function of the Cd's depth. In effect, using the VASP (WIEN2K) code we predict  $V_{33} = 4.96(5.25) \times 10^{21}$  V/m<sup>2</sup>,  $5.67(5.99) \times 10^{21}$  V/m<sup>2</sup>, and  $1.91(1.83) \times 10^{21}$  V/m<sup>2</sup> for InCd<sub>1</sub>, InCd<sub>2</sub>, and InCd<sub>16</sub> systems, respectively.

We present herein the predicted EFG tensor results at the Cd site located substitutionally at each inequivalent In site in the reconstructed In(111) surface, after each Cd-doped system achieved its equilibrium structure. In Fig. 9 we show the behavior of the predicted EFG tensor as a function of the depth of the Cd impurity from the surface. In Fig. 9(a) we show the predicted results obtained with VASP for  $V_{11}$ ,  $V_{22}$ , and  $V_{33}$ , showing that all EFG components are converged for Cd atoms located deeper than 6.5 Å from the surface. Moreover,

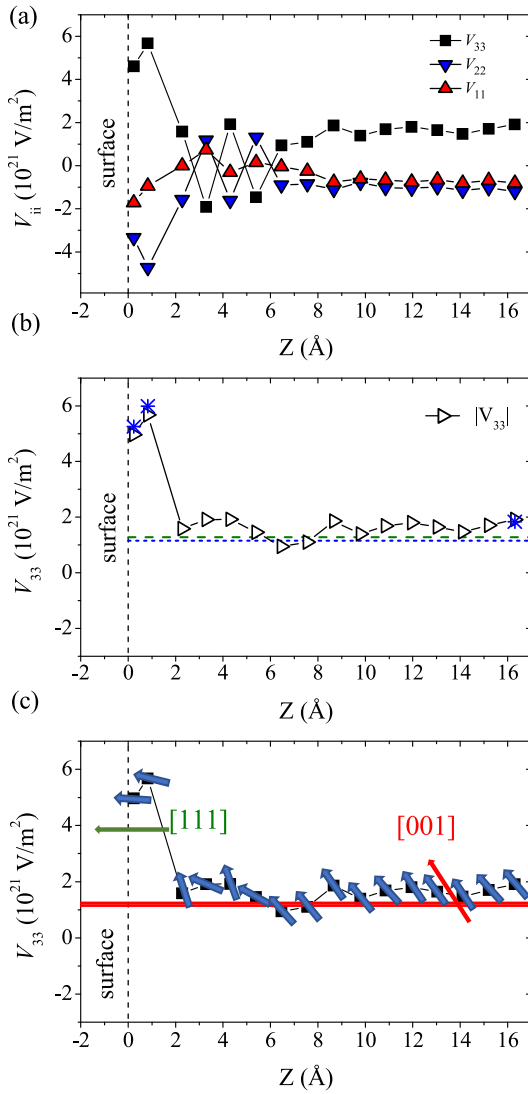


FIG. 9. (a) Predicted EFG components at the Cd site as a function of the depth of the Cd atom from the In(111) surface. (b) Comparison of predicted  $|V_{33}|$  (white triangles) at the Cd site as a function of the depth of the Cd atom from the (111) surface with the *ab initio* prediction of  $V_{33}$  in Cd-doped In bulk by VASP (green dashed line) and WIEN2K (blue dotted line). The  $V_{33}$  predictions by WIEN2K (blue star) for In: Cd<sub>1</sub>, In: Cd<sub>2</sub>, and In: Cd<sub>16</sub>, are also indicated. (c) Comparison of  $V_{33}$  direction at the Cd site as a function of the depth of the Cd atom from the In(111) surface with the experimental  $V_{33}$  direction at <sup>111</sup>Cd related with HFI<sup>B</sup> (red arrow) and HFI<sup>S</sup> (green arrow). The red solid line represents the experimental value of  $V_{33}$  at the <sup>111</sup>Cd site in In bulk (see Table I) [37,41,47].  $Z = 0 \text{ \AA}$  is the position of the topmost In atom in each reconstructed Cd-doped In(111) surface.

$V_{11}$  and  $V_{22}$  tend to the same value, indicating that the EFG tensor recovers the axial symmetry ( $\eta \rightarrow 0$ ) that it has when the Cd impurity is located at the substitutional In site in bulk indium [41,47].

In Fig. 9(b) we show the predictions of  $V_{33}$  and  $|V_{33}|$  at the Cd site as a function of the depth of the Cd atom from the reconstructed (111) surface. Here we compare these predictions to our prediction of  $V_{33}$  in In bulk. As this figure

TABLE I. TDPAC experimental  $V_{33}$  results at the (<sup>111</sup>In  $\rightarrow$ )<sup>111</sup>Cd site in indium bulk, taken at  $T = 1.2 \text{ K}$ ,  $4.2 \text{ K}$  [41], and  $77 \text{ K}$  [37,41,47]. The quadrupole moment of the  $I = +5/2$  intermediate nuclear state of <sup>111</sup>Cd,  $Q = +0.76(2) \text{ b}$  [60], was used to obtain  $V_{33}$ , assuming a positive sign for the quadrupole frequency in accordance with the *ab initio* predictions. The errors in  $V_{33}$  take into account also the  $Q$  error and the  $\eta = 0$  values were kept fixed during the fitting procedure.

$V_{33}$ ( $10^{21} \text{ V/m}^2$ )	$\eta$	$T$ (K)
1.35 (4)	0	1.2 <sup>a</sup>
1.37 (4)	0	4.2 <sup>a</sup>
1.34 (4)	0	77 <sup>a</sup>
1.32 (4)	0	77 <sup>b</sup>
1.33 (4)	At least $<0.1$	77 <sup>c</sup>

<sup>a</sup>Reference [41].

<sup>b</sup>Reference [47].

<sup>c</sup>Reference [37].

shows, for Cd atoms located deeper than  $6 \text{ \AA}$  from the surface,  $V_{33}$  tends to recover the bulk value predicted both by WIEN2K and VASP. Nevertheless,  $|V_{33}|$ , which is the observable in standard TDPAC experiments, recovers its bulk value immediately below the surface (see the white triangles), having an average of  $\langle |V_{33}| \rangle = 1.6 \times 10^{21} \text{ V/m}^2$ , with a standard deviation of  $0.3 \times 10^{21} \text{ V/m}^2$ , in excellent agreement with the *ab initio* simulated bulk value (see solid blue and dashed green lines).

The red solid line in Fig. 9(c) represents the experimental values of  $V_{33}$  at the <sup>111</sup>Cd site in the In bulk. In Table I the experimental  $V_{33}$  determinations by different authors and temperatures are quoted [37,41,47]. Again, in these experiments the  $V_{33}$  orientation was not determined. In summary, the predicted values for the deeper Cd atoms from the (111) surface are in excellent agreement with those predicted for Cd localized at the substitutional In site in bulk (by VASP and WIEN2K) and with those reported experimentally for <sup>111</sup>Cd localized at In sites in indium bulk. With respect to the predicted  $V_{33}$  direction at the Cd site, we can see in Fig. 9(c) that this component is perpendicular to the (111) surface for the two most superficial Cd atoms. For the rest of the Cd atoms,  $V_{33}$  is oriented along the [001] direction (which is our predicted orientation in Cd-doped In bulk), except for In: Cd<sub>4</sub> and In: Cd<sub>6</sub> systems where it is a little bit tilted. Both predicted directions are in excellent agreement with those reported experimentally for HFI<sup>S</sup> and HFI<sup>B</sup>, respectively [29]. In view of the lack of experimental determination of  $V_{33}$  orientation in <sup>111</sup>Cd-doped In bulk, our prediction for this observable provides essential support to the assignment of HFI<sup>B</sup> to <sup>111</sup>Cd probes localized in a bulklike environment in the In thin film.

Now we will discuss in more detail the differences between the behavior of the EFG near the surface in the pure In(111) and the Cd-doped In(111) surfaces, in order to understand the origin of these differences. For the Cd-doped In(111) surfaces, as shown in Fig. 9(b),  $|V_{33}|$  at the Cd site in In: Cd<sub>1</sub> and In: Cd<sub>2</sub> systems has a higher value (around 4 times) than the one predicted at the Cd atom in the rest of the In: Cd<sub>*i*</sub> ( $i = 3$  to 16) surfaces. On the other hand, for the undoped reconstructed

In(111) surface, as shown in Fig. 5(b),  $|V_{33}|$  presents a large value only at the In atom located just below the surface ( $\text{In}_2$ ), while at the topmost  $\text{In}_1$  atom  $|V_{33}|$  has a low value like in the bulk.

In order to separate the structural and electronic effects we took the reconstructed undoped In(111) surface, replacing the  $\text{In}_1$  atom by a Cd atom, and then the EFG was calculated at the Cd site at these fixed atomic positions. We found a value of  $V_{33} = 3.94 \times 10^{21} \text{ V/m}^2$ , similar to the value at the  $\text{In}_1$  site in the reconstructed pure (111) surface  $V_{33} = 3.42 \times 10^{21} \text{ V/m}^2$ . On the other hand, we took the equilibrium structure found in the In:Cd<sub>1</sub> system, replacing the Cd atom (topmost Cd atom) by an In one, and then calculating the EFG at the Cd site at these fixed atomic positions. This time we found a value of  $V_{33} = 4.76 \times 10^{21} \text{ V/m}^2$ , similar to the value at the Cd site in In:Cd<sub>1</sub> system,  $V_{33} = 4.96 \times 10^{21} \text{ V/m}^2$ . This shows that the little differences between the electronic configurations of In and Cd are not responsible for the difference in the  $V_{33}$  values at In and Cd atoms localized at the topmost site in the (111) surface.

At this point, a structural effect seems to be responsible for the increase in the  $V_{33}$  value when the topmost In atom is replaced by a Cd atom (i.e., the In:Cd<sub>1</sub> system). In effect, inspecting Fig. 8 (first panel), we can see that the distances to all nearest In neighbors from Cd ( $d_{\text{NN}}$ ) decrease when the topmost In atom is replaced by Cd and the In:Cd<sub>1</sub> system reaches its equilibrium structure. Therefore, we could understand this increase in  $V_{33}$  due to the strong EFG dependence upon  $r^{-3}$  from the charge sources. In our system, the completely filled  $d$  shell in the Cd atoms does not contribute to the EFG. Again, as discussed for the pure surfaces, we will analyze only the contribution to the EFG from the  $p$  electrons, computing the  $p$  electrons' asymmetry count  $\Delta n_p$ . The decrease in  $d_{\text{NN}}$  for the In:Cd<sub>1</sub> system mentioned before could increase the electronic charge density along the Cd-In<sub>NN</sub> bonds and if this increment, due to the Cd's coordination geometry, is larger in the plane normal to  $V_{33}$  compared to the electronic density variation along the  $V_{33}$  direction, the  $V_{33}$  value will increase. In effect, numerical evaluation of  $n_{p_i}$  at the Cd site supports this scenario, explaining the increase of  $V_{33}$  at the topmost site when Cd replaces the In site in the undoped In(111) surface.

In the framework of the precedent analyses, we showed that at the surface (i.e., for Cd localized in In:Cd<sub>1</sub> and In:Cd<sub>2</sub>) the electronic charges of Cd  $5p$  electrons are basically distributed in the (111) plane, and when the Cd is sunken into the bulk, this charge becomes axially symmetric in a plane normal to the [001] direction and its contribution to  $V_{33}$  becomes similar to the contribution of the charge distributed along the [001] direction.

In summary, for the Cd-doped (111) surface, we predicted basically two very different EFG tensors (in magnitude and direction) depending on the Cd atom's depth from the surface, one at the Cd atoms located in In:Cd<sub>1</sub> and In:Cd<sub>2</sub> systems, i.e., at the two most superficial substitutional In sites, and the other at the Cd atoms located beyond 6 Å (In : Cd<sub>7-16</sub>). The comparison between these predicted EFGs with the TDPAC experimental results reported by Körner *et al.* [29] will be done in the next section together with a deep discussion on the origin of the EFGs at  $^{111}\text{Cd}$  probes measured in these grown *layer-by-layer*<sup>111</sup>In-doped In surfaces.

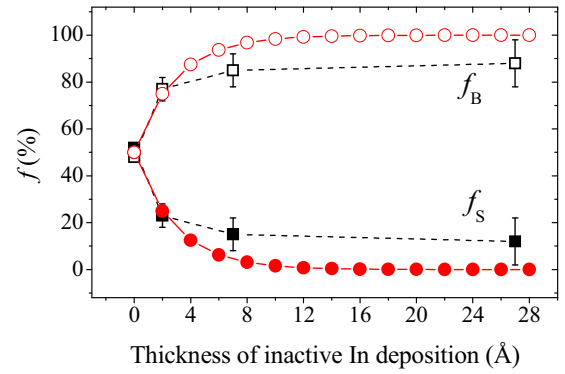


FIG. 10. Experimental [29] (squares) and predicted (circles) fractions  $f_S$  (filled symbols) and  $f_B$  (hollow symbols) as a function of the thickness of inactive In deposition.

#### IV. DISCUSSION

As mentioned in the Introduction section, Körner *et al.* [29] reported only two hyperfine interactions in their TDPAC experiments, called  $\text{HFI}^S$  and  $\text{HFI}^B$ . Both interactions are well resolved, with hyperfine parameters independent from the deposited inactive In layers on the active one, but with fractions monotonously variable as a function of thickness of inactive In deposition.

Figure 10 shows  $\text{HFI}^S$  and  $\text{HFI}^B$  experimental fractions (squares) as a function of the thickness of deposited inactive In. From the decrease of  $\text{HFI}^S$  as the thickness of deposited inactive In increases (and vice versa for  $\text{HFI}^B$ ), and in addition due to the fact that the EFG from  $\text{HFI}^B$  is in excellent agreement with the experimental EFG at  $^{111}\text{Cd}$  sites in bulk indium [Fig. 9(c) and Table I], Körner *et al.* [29] assigned  $\text{HFI}^S$  and  $\text{HFI}^B$  to  $^{111}\text{Cd}$  probes localized at “the surface” and at “the bulk,” respectively. The surface is defined as an active layer 3 Å thick (on average), called a “monolayer,” without any inactive layer on it [see Fig. 11(a), top]. The bulk in their scenario was defined as one active monolayer with another active monolayer on it [see Fig. 11(a), top], i.e., an active (6-Å-thick) “bilayer,” since  $\text{HFI}^B$  was already observed in the first experiment in which only active In:<sup>111</sup>In was deposited on the In substrate and because they assumed that in a 3-Å-thick active monolayer there only exist ( $^{111}\text{In} \rightarrow$ )<sup>111</sup>Cd probes sensing  $\text{HFI}^S$ . In the successive experiments, the bulk was defined as the active layer (mono- or bilayer) with one or more inactive layers on it; the situation is illustrated in Fig. 11(a) (middle and bottom).

The fact that both experimental EFGs are well resolved, the agreement of  $V_{33}^B$  with the experimental EFG at  $^{111}\text{Cd}$ -doped In bulk, and the well-known  $r^{-3}$  EFG dependence from the charge sources should imply that the EFG is governed by the electronic charge distribution within a monolayer (or less). In the same way, the atomic positions should converge to the bulk ones inside this monolayer. In another way, intermediate  $V_{33}$  values between  $V_{33}^S$  and  $V_{33}^B$  should have been observed as the inactive layers are deposited.

In Fig. 12, the zones between the horizontal dashed black lines represent the experimental  $V_{33}$  values of  $\text{HFI}^S$  and  $\text{HFI}^B$  obtained using  $Q^{111}\text{Cd}(I = +5/2) = 0.76(2)$  b [60] taking into account the error bar in the  $Q$  value and the fitting

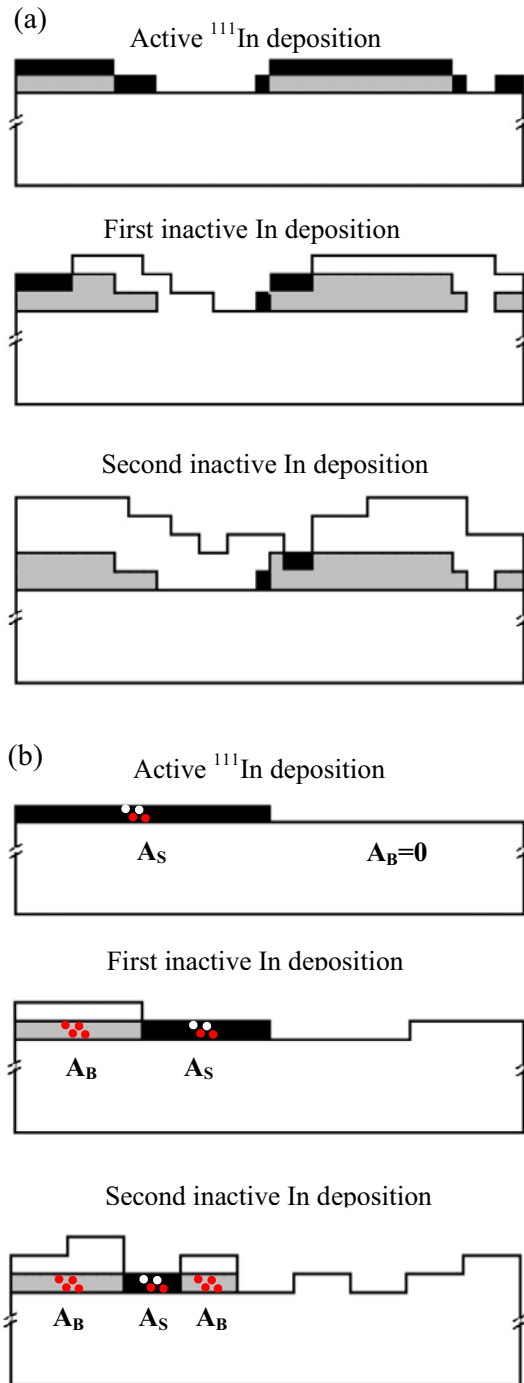


FIG. 11. (a) Deposition model proposed by Körner *et al.* [29] to interpret the experimental results shown in Figs. 10 and 12. In this model, the black area represents the layers with ( $^{111}\text{In} \rightarrow$ )  $^{111}\text{Cd}$  probes sensing  $\text{HFI}^{\text{S}}$ , the gray area represents the layers with probes sensing  $\text{HFI}^{\text{B}}$ , and the white area represents the inactive layers and the In substrate. (b) Deposition model proposed in this work (see text for details). The black and gray areas represent active monolayers doped with  $^{111}\text{In}$ , and the white areas represent inactive layers and the In substrate.  $A_{\text{S}}$  is the area containing one active monolayer with  $^{111}\text{Cd}$  localized at two sites (white dots) sensing  $\text{HFI}^{\text{S}}$  and at two sites (red dots) sensing  $\text{HFI}^{\text{B}}$ .  $A_{\text{B}}$  is the area containing one active monolayer with  $^{111}\text{Cd}$  localized at four sites sensing  $\text{HFI}^{\text{B}}$ .

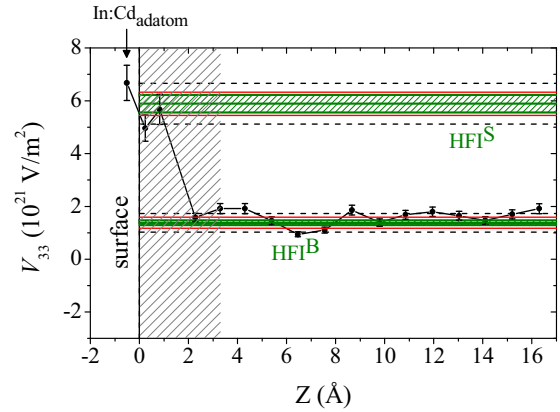


FIG. 12. Comparison between experimental  $|V_{33}|$  values (horizontal regions) related to  $\text{HFI}^{\text{S}}$  and  $\text{HFI}^{\text{B}}$  with the *ab initio* predictions (black points, with precision errors) at Cd sites as a function of the depth of the Cd atom from the In(111) surface. The region between horizontal (black) dashed lines represents the experimental  $|V_{33}|$  (the  $V_{33}$  sign cannot be determined in a TDPAC experiment such as that of Ref. [29]) taking into account the fit uncertainty in  $\omega_0$  and the quadrupole moment  $Q$  error (green dashed region), and the frequency distribution (region between red lines). The  $V_{33}$  prediction for the adatom site is also indicated. The dashed black vertical region represents the situation of  $^{111}\text{Cd}$  probes at the active monolayer of the model proposed in this work, before the inactive In deposition [see Fig. 11(b), top].

error (green lines) and the EFG distribution (red lines). In the *ab initio* predictions (black points), the nominal precision error usually ascribed [60] to APW calculations of the EFG was also indicated. Comparing the  $V_{33}$  predictions to the experimental  $V_{33}$  values of  $\text{HFI}^{\text{S}}$  and  $\text{HFI}^{\text{B}}$  we see that  $\text{HFI}^{\text{B}}$  already exists within one active monolayer. From the ratio of the experimental fractions of  $^{111}\text{Cd}$  probes sensing  $\text{HFI}^{\text{S}}$  and  $\text{HFI}^{\text{B}}$  when no inactive In was deposited, we proposed a thickness of 3.28 Å (black dashed region in Figs. 12, with four nonequivalent In sites along the  $z$  direction) for the active monolayer, in which there exist two sites sensing  $\text{HFI}^{\text{S}}$  and two sites sensing  $\text{HFI}^{\text{B}}$ , in agreement with the equal populations of both interactions (see Fig. 10).

Let us discuss the rather large experimental EFG distributions observed for  $\text{HFI}^{\text{S}}$  and  $\text{HFI}^{\text{B}}$ . The 15% EFG distribution of  $\text{HFI}^{\text{B}}$ , already seen in the first experiment in which only the active layer was deposited, is compatible with the difference between the predicted  $V_{33}$  at Cd sites in In: $\text{Cd}_3$  and In: $\text{Cd}_4$  systems (see Fig. 12). For the rest of the experiments with additional deposited inactive layers, this EFG distribution is also compatible with the difference between the predicted  $V_{33}$  values for four successive (along the  $Z$  direction) Cd sites. On the other hand, the 7% EFG distribution of  $\text{HFI}^{\text{S}}$  is compatible with the difference between our predicted  $V_{33}$  at Cd sites in In: $\text{Cd}_1$  and In: $\text{Cd}_2$  systems.

In their work, Körner *et al.* [29] proposed a scenario in which after the  $^{111}\text{In}$  deposition there exist some zones in the sample only with the backing substrate, zones with a 3-Å active monolayer and zones with active bilayers. Taking into account the excellent agreement between the *ab initio* predictions and the experimental EFGs coming from  $\text{HFI}^{\text{S}}$  and  $\text{HFI}^{\text{B}}$ , their fractions when no inactive In atoms are deposited

(first experiment), and the precedent analysis of the EFG distributions, we propose a model consisting in one monolayer deposition discarding the necessity of having an active bilayer to observe a bulk signal in the first experiment.

As we have seen before, the proposed monolayer of  $3.28 \text{ \AA}$  thickness has, for this active monolayer, two sites sensing  $\text{HFI}^{\text{S}}$  and two sites sensing  $\text{HFI}^{\text{B}}$ , and when inactive In is deposited over it, the four sites sense  $\text{HFI}^{\text{B}}$ . Hence, after the deposition of this proposed active monolayer, the fractions of probes that sense  $\text{HFI}^{\text{S}}$  and  $\text{HFI}^{\text{B}}$  are equal, in agreement with the first experiment. A combination of active monolayers and bilayers would present a higher fraction for  $\text{HFI}^{\text{B}}$ , not compatible with the first experiment. At this point we can say that the In depositions do not cover the whole sample because in this case, after the first inactive deposition, all the  $^{111}\text{Cd}$  probes would sense  $\text{HFI}^{\text{B}}$ . but it is not possible to determine yet the relative surface cover by the deposition.

For this, we calculate the fraction  $f_{\text{S}}$  of  $^{111}\text{Cd}$  probes that sense  $\text{HFI}^{\text{S}}$  in any of these experiments. Counting the number of sites that sense  $\text{HFI}^{\text{S}}$  with respect to the total number of sites occupied by  $^{111}\text{Cd}$  probes in any of the configurations of In deposition [see Fig. 11(b), middle and bottom], this leads to  $f_{\text{S}} = \frac{2A_{\text{S}}}{4(A_{\text{S}}+A_{\text{B}})} = \frac{2}{4(1+\frac{A_{\text{B}}}{A_{\text{S}}})}$ , where  $A_{\text{S}}$  is the area of the sample surface only covered with the active monolayer (i.e., without any inactive monolayer on it) and  $A_{\text{B}}$  is the area of the active monolayer covered by at least one inactive In layer in the subsequent experiments. To construct  $f_{\text{S}}$  we took into account that the active  $A_{\text{S}}$  monolayer contributes with  $2A_{\text{S}}$  sites sensing  $\text{HFI}^{\text{S}}$  and  $2A_{\text{S}}$  sites sensing  $\text{HFI}^{\text{B}}$  [i.e., when the active monolayer does not have any inactive layer on it; see black area in Fig. 11(b)]. On the other hand, the active  $A_{\text{B}}$  layer contributes with  $4A_{\text{B}}$  sites sensing  $\text{HFI}^{\text{B}}$ . The total number of active sites in the whole area of the active layer is  $4(A_{\text{S}} + A_{\text{B}})$ . *A priori* the relation between  $A_{\text{S}}$  and  $A_{\text{B}}$  is not known for each deposition. If we suppose that each In (inactive) deposition covers *half* the surface covered in the previous deposition, we predict  $f_{\text{S}}$  and  $f_{\text{B}}$  shown by the red circles in Fig. 10, in very good agreement with the experimental ones (black squares in Fig. 10). As the first inactive layer deposited has an average of  $2 \text{ \AA}$ , we supposed for constructing this plot (circles) that each subsequent inactive deposition also has  $2 \text{ \AA}$  in average. It should be noted that an experimental null fraction for  $\text{HFI}^{\text{S}}$  should be expected after  $27 \text{ \AA}$  of inactive In deposition. Although the observed fraction is null taking into account the experimental error bar that comes from the fitting procedure, the only explanation for a remaining fraction of  $\text{HFI}^{\text{S}}$  is that a little uncovered surface should remain in the deposition process between  $7$  and  $27 \text{ \AA}$ , a process that was not explained in detail in Ref. [29].

In other metallic surfaces, also doped with ( $^{111}\text{In} \rightarrow$ )  $^{111}\text{Cd}$  impurities, adatom sites have been reported in a theoretical work by Cottenier *et al.* [40], in which DFT-based EFG predictions and TDPAC results were compared. In these samples, the fraction of probes assigned to adatom sites decreases after thermal treatments, in favor of surface sites. The  $V_{33}$  value at the adatom site is predicted to be smaller than at the surface site. This behavior was explained as a function of the nearest neighbor coordination number (NN), with  $V_{33}$  increasing as NN increases. In order to explore the possible

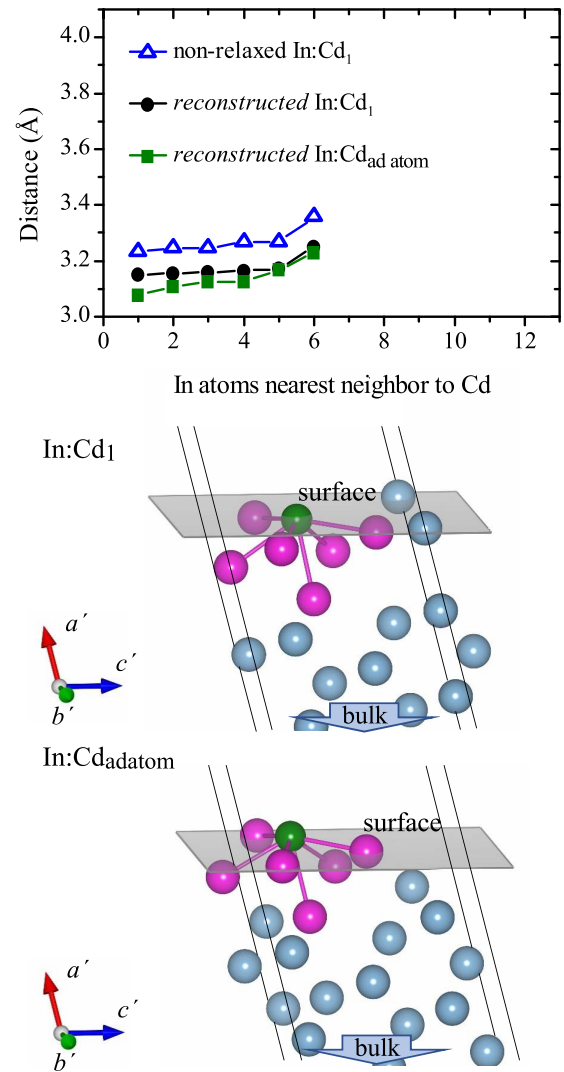


FIG. 13. At the top, Cd- $\text{In}_{\text{NN}}$  bond lengths for the nonrelaxed (blue triangles) and reconstructed (black circles)  $\text{In}:\text{Cd}_1$  systems, and reconstructed Cd- $\text{In}_{\text{NN}}$  bond lengths for the  $\text{In}:\text{Cd}_{\text{adatom}}$  system (green squares). The  $\text{In}_{\text{NN}}$  atoms are arbitrarily labeled in the horizontal axis. Cd (in green) coordination with its nearest In neighbors (in magenta) in the  $\text{In}:\text{Cd}_1$  (middle) and  $\text{In}:\text{Cd}_{\text{adatom}}$  (bottom) systems. The gray plane represents the  $\text{In}(111)$  surface and the light blue spheres the deeper In atoms.

existence of this defect, we perform *ab initio* calculations for the  $\text{In}(111)$  surface localizing a Cd atom in an adatom site, using the same procedure as in the rest of the doped systems described before. After full relaxation of this doped system, we obtained the  $V_{33}$  value shown in Fig. 12. As was done for the  $\text{In}:\text{Cd}_1$ ,  $\text{In}:\text{Cd}_2$ , and  $\text{In}:\text{Cd}_{16}$  systems, we used WIEN2K to obtain equilibrium structures starting from the atomic equilibrium positions obtained with VASP. We performed this additional check for this atomic site since this is not a crystalline position. The results of  $V_{33}$  and its direction are almost the same with both methods. The EFG prediction at the adatom is in good agreement with the experimental  $V_{33}$  related with  $\text{HFI}^{\text{S}}$ , as shown in Fig. 12. In our case, the adatom  $V_{33}$  has a similar value to  $V_{33}$  at the surface sites ( $\text{In}:\text{Cd}_1$  and  $\text{In}:\text{Cd}_2$  systems). At this point it is important to

mention that in the surfaces studied in Ref. [40] the EFGs in the bulk systems are null due to the high symmetry of the fcc unit cell, very different from the tetragonal crystal structure of In. Also, and more important, the coordination number of the adatom and the topmost surface site (In:Cd<sub>1</sub>) in the In(111) surface are both NN = 6 and their coordination geometry is very similar, as shown in Fig. 13, with the Cd-In<sub>i</sub> bond lengths slightly shorter for the adatom site. All these features explain the slightly higher  $V_{33}$  value at the adatom site. Comparing the experimental  $V_{33}$  from HFI<sup>S</sup> and the *ab initio* predictions, we cannot discard the presence of <sup>111</sup>Cd atoms at adatom sites. If the adatom site and the surface ones are equally populated, the fraction of probes sensing HFI<sup>S</sup> would be 60%, in disagreement with the experimental result of the same experiment. <sup>111</sup>In being indistinguishable from the rest of the In atoms of the surface, the probability to have an adatom is much less than in the case in which the <sup>111</sup>In probe is an impurity deposited on a surface. A low percentage of <sup>111</sup>Cd atoms in adatom sites can be possible and compatible with the experimental EFG distribution observed and would lead to a ratio of fractions slightly different from unity and closer to the experimental value ( $f_S/f_B = 1.083$ ).

## V. CONCLUSIONS

In this paper we presented a comprehensive work explaining the behavior of the electric field gradient (EFG) at pure In(111) and Cd-doped In(111) surfaces. In order to separate the effects produced by the surface generation and the presence of the impurity, we studied in addition the pure and Cd-doped In bulk. We provided theoretical information from first principles to explain previously performed TDPAC experiments at <sup>111</sup>Cd impurity probe atoms, obtained by depositing <sup>111</sup>In isotopes onto an In(111) surface of thin films under ultrahigh vacuum, afterwards adding inactive indium layer by layer onto it. In this sense we confirmed the existence of *only* two hyperfine interactions (instead of a possible continuous set of  $V_{33}$  as the probe “goes” deeper from the surface into the bulk), one related with <sup>111</sup>Cd probes localized at the two more superficial In sites (HFI<sup>S</sup>) and the other related with probes localized at any of the other inequivalent In sites existing from the surface towards the bulk (HFI<sup>B</sup>), in excellent agreement with the experimental  $V_{33}$ , both in magnitude and direction. In the case of HFI<sup>S</sup>,  $V_{33}$  is oriented normal to the (111) surface, and for HFI<sup>B</sup> we found a  $V_{33}$  orientation parallel to the [001] axis and coincident with the orientation predicted for both the pure and Cd-doped In bulk, in agreement with the experi-

mental orientation reported for HFI<sup>B</sup>. Our prediction of this last orientation enabled us to confirm the good assignment of HFI<sup>B</sup> since the experimental determination of the  $V_{33}$  direction has not been determined yet in bulk samples. In addition, we showed that the axial symmetry that the EFG has in pure and Cd-doped In bulk systems is recovered in a pure or Cd-doped thin film as the probe (In or Cd, respectively) goes deeper from the surface into the bulk. We also showed that the breaking of the bulk axial symmetry is already observed in the just generated surface.

With respect to the EFG behavior at and close to the pure and Cd-doped In(111) surface we could separate the structural and electronic effects and their sources. The pure system enabled us to show the structural modifications introduced by the surface generation itself and to explain the high  $V_{33}$  value found for the In<sub>2</sub> site (the one below the topmost In atom at the surface) in terms of the bond-length relaxations and redistribution of the electronic density around the probe atom. When the Cd impurity is introduced in the surface at the topmost In site, only a structural effect produces the increase of  $V_{33}$  leading to the experimental ratio  $|V_{33}^S/V_{33}^B| \approx 4$ . These light structural modifications have an important impact on the Cd *p*-states distribution, which governs the  $V_{33}$  behavior.

Finally, from the combination of the predicted  $V_{33}$  for the Cd-doped systems as a function of the depth of the Cd localization from the surface with the fractions of HFI<sup>S</sup> and HFI<sup>B</sup> observed in the TDPAC experiment performed before the inactive In deposition, we demonstrated that a single 3-Å active In monolayer deposited onto the In(111) surface was enough to explain the origin of these fractions, in discrepancy with the previous interpretation of the experiments. Within this scenario we proposed a deposition rate for the inactive In layers that is in agreement with the experimental fraction evolution of HFI<sup>S</sup> and HFI<sup>B</sup> as a function of inactive In deposition.

## ACKNOWLEDGMENTS

This work was partially supported by Consejo Nacional de Investigaciones Científicas y Técnicas (CONICET), Argentina, under Grants No. PIP0002 and PIP0803. M.R. and G.N.D. acknowledge support as CONICET and UNLP fellows. This research made use of the computational facilities of the Physics of Impurities in Condensed Matter (PhI) group at IFLP and Departamento de Física (UNLP). R.F. acknowledges the support of the Uruguayan organizations PEDECIBA, CSIC, and ANII.

- [1] A. Lerf and T. Butz, *Angew. Chem., Int. Ed. Engl.* **26**, 110 (1987).
- [2] R. Vianden and U. Feuser, *Phys. Rev. Lett.* **61**, 1981 (1988).
- [3] N. Achtziger and W. Witthuhn, *Phys. Rev. B* **47**, 6990 (1993).
- [4] M. Uhrmacher, R. N. Attili, K. P. Lieb, K. Winzer, and M. Mekata, *Phys. Rev. Lett.* **76**, 4829 (1996).
- [5] J. Luthin, K. P. Lieb, M. Neubauer, M. Uhrmacher, and B. Lindgren, *Phys. Rev. B* **57**, 15272 (1998).
- [6] R. N. Attili, R. N. Saxena, A. W. Carbonari, J. Mestnik Filho, M. Uhrmacher, and K. P. Lieb, *Phys. Rev. B* **58**, 2563 (1998).

- [7] S. Lany, P. Blaha, J. Hamann, V. Ostheimer, H. Wolf, and T. Wichert, *Phys. Rev. B* **62**, R2259 (2000).
- [8] J. Meersschaut, C. L’abbé, M. Rots, and S. D. Bader, *Phys. Rev. Lett.* **87**, 107201 (2001).
- [9] L. A. Errico, G. Fabricius, M. Rentería, P. de la Presa, and M. Forker, *Phys. Rev. Lett.* **89**, 055503 (2002).
- [10] M. Forker, S. Müller, P. de la Presa, and A. F. Pasquevich, *Phys. Rev. B* **68**, 014409 (2003).
- [11] J. M. Ramallo-López, M. Rentería, E. E. Miró, F. G. Requejo, and A. Traverse, *Phys. Rev. Lett.* **91**, 108304 (2003).

- [12] A. W. Carbonari, J. Mestnik-Filho, R. N. Saxena, and M. V. Lalić, *Phys. Rev. B* **69**, 144425 (2004).
- [13] M. Forker, P. de la Presa, W. Hoffbauer, S. Schlabach, M. Bruns, and D. V. Szabó, *Phys. Rev. B* **77**, 054108 (2008).
- [14] G. N. Darriba, L. A. Errico, P. D. Eversheim, G. Fabricius, and M. Rentería, *Phys. Rev. B* **79**, 115213 (2009).
- [15] H. Jaeger and M. O. Zacate, *Defect and Diffusion Studied Using PAC Spectroscopy* (Trans Tech Publications Ltd., Zurich, Switzerland, 2011).
- [16] S. Zhu, G. Zhang, F. Li, and D. Yuan, in *Proceedings of the 4th Joint International Conference on Hyperfine Interactions and International Symposium on Nuclear Quadrupole Interactions* (Springer, Dordrecht, Netherlands, 2013).
- [17] F. H. M. Cavalcante, O. F. L. S. Leite Neto, H. Saitovitch, J. T. P. D. Cavalcante, A. W. Carbonari, R. N. Saxena, B. Bosch-Santos, L. F. D. Pereira, J. Mestnik-Filho, and M. Forker, *Phys. Rev. B* **94**, 064417 (2016).
- [18] L. A. Terrazos, H. M. Petrilli, M. Marszalek, H. Saitovitch, P. R. J. Silva, P. Blaha, and K. Schwarz, *Solid State Commun.* **121**, 525 (2002).
- [19] L. A. Errico, G. Fabricius, and M. Rentería, *Phys. Rev. B* **67**, 144104 (2003).
- [20] G. N. Darriba, M. Rentería, H. M. Petrilli, and L. V. C. Assali, *Phys. Rev. B* **86**, 075203 (2012).
- [21] M. Forker, P. R. J. Silva, J. T. P. D. Cavalcante, F. H. M. Cavalcante, S. M. Ramos, H. Saitovitch, E. Baggio-Saitovitch, R. Alonso, M. Taylor, and L. A. Errico, *Phys. Rev. B* **87**, 155132 (2013).
- [22] G. N. Darriba, E. L. Muñoz, L. A. Errico, and M. Rentería, *J. Phys. Chem. C* **118**, 19929 (2014).
- [23] R. R. do Nascimento, F. C. D. A. Lima, M. B. Gonçalves, L. A. Errico, M. Rentería, and H. M. Petrilli, *J. Mol. Model.* **21**, 97 (2015).
- [24] C. Sena, M. S. Costa, E. L. Muñoz, G. A. Cabrera-Pasca, L. F. D. Pereira, J. Mestnik-Filho, A. W. Carbonari, and J. A. H. Coaquira, *J. Magn. Magn. Mater.* **387**, 165 (2015).
- [25] D. Richard, G. N. Darriba, E. L. Muñoz, L. A. Errico, P. D. Eversheim, and M. Rentería, *J. Phys. Chem. C* **120**, 5640 (2016).
- [26] G. N. Darriba, E. L. Muñoz, A. W. Carbonari, and M. Rentería, *J. Phys. Chem. C* **122**, 17423 (2018).
- [27] P. Hohenberg and W. Kohn, *Phys. Rev.* **136**, B864 (1964).
- [28] W. Kohn and L. J. Sham, *Phys. Rev.* **140**, A1133 (1965).
- [29] W. Körner, W. Keppner, B. Lehdorff-Junges, and G. Schatz, *Phys. Rev. Lett.* **49**, 1735 (1982).
- [30] T. Klas, J. Voigt, W. Keppner, R. Wesche, and G. Schatz, *Phys. Rev. Lett.* **57**, 1068 (1986).
- [31] T. Klas, R. Fink, G. Krausch, R. Platzter, J. Voigt, R. Wesche, and G. Schatz, *Europhys. Lett.* **7**, 151 (1988).
- [32] T. Klas, R. Fink, G. Krausch, R. Platzter, J. Voigt, R. Wesche, and G. Schatz, *Surf. Sci.* **216**, 270 (1989).
- [33] R. Wesche, R. Fink, T. Klas, G. Krausch, R. Platzter, J. Voigt, and G. Schatz, *J. Phys.: Condens. Matter* **1**, 7407 (1989).
- [34] R. Fink, R. Wesche, T. Klas, G. Krausch, R. Platzter, J. Voigt, U. Wöhrmann, and G. Schatz, *Surf. Sci.* **225**, 331 (1990).
- [35] E. Hunger and H. Haas, *Surf. Sci.* **234**, 273 (1990).
- [36] R. Fink, B.-U. Runge, K. Jacobs, G. Krausch, J. Lohmüller, B. Luckscheiter, U. Wöhrmann, and G. Schatz, *J. Phys.: Condens. Matter* **5**, 3837 (1993).
- [37] E. Bodenstedt, U. Ortabasi, and W. H. Ellis, *Phys. Rev. B* **6**, 2909 (1972).
- [38] K. Potzger, A. Weber, H. H. Bertschat, W.-D. Zeitz, and M. Dietrich, *Phys. Rev. Lett.* **88**, 247201 (2002).
- [39] D. Wiarda, M. Uhrmacher, A. Bartos, and K. P. Lieb, *J. Phys.: Condens. Matter* **5**, 4111 (1993).
- [40] S. Cottenier, V. Bellini, M. Çakmak, F. Manghi, and M. Rots, *Phys. Rev. B* **70**, 155418 (2004).
- [41] J. Christiansen, P. Heubes, R. Keitel, W. Klinger, W. Loeffler, W. Sandner, and W. Witthuhn, *Z. Phys. B* **24**, 177 (1976).
- [42] F. C. Thatcher and R. R. Hewitt, *Phys. Rev. B* **1**, 454 (1970).
- [43] W. D. Brewer and G. Kaindl, *Hyperfine Interact.* **4**, 576 (1978).
- [44] W. W. Simmons and C. P. Slichter, *Phys. Rev.* **121**, 1580 (1961).
- [45] R. R. Hewitt and T. T. Taylor, *Phys. Rev.* **125**, 524 (1962).
- [46] W. J. O'Sullivan and J. E. Schirber, *Phys. Rev.* **135**, A1261 (1964).
- [47] C. Budtz-Jørgensen and K. B. Nielsen, *Hyperfine Interact.* **1**, 81 (1975).
- [48] M. Wolcyrz, R. Kubiak, and S. Maciejewski, *Phys. Status Solidi B* **107**, 245 (1981).
- [49] G. Kresse and J. Furthmüller, *Phys. Rev. B* **54**, 11169 (1996).
- [50] G. Kresse and J. Furthmüller, *Comput. Mater. Sci.* **6**, 15 (1996).
- [51] G. Kresse and J. Hafner, *Phys. Rev. B* **47**, 558 (1993).
- [52] G. Kresse and J. Hafner, *Phys. Rev. B* **49**, 14251 (1994).
- [53] G. Kresse and D. Joubert, *Phys. Rev. B* **59**, 1758 (1999).
- [54] P. E. Blöchl, *Phys. Rev. B* **50**, 17953 (1994).
- [55] J. P. Perdew, K. Burke, and M. Ernzerhof, *Phys. Rev. Lett.* **77**, 3865 (1996).
- [56] G. K. H. Madsen, P. Blaha, K. Schwarz, E. Sjöstedt, and L. Nordström, *Phys. Rev. B* **64**, 195134 (2001).
- [57] P. Blaha, K. Schwarz, G. Madsen, D. Kvasnicka, and J. Luitz, *WIEN2K, an Augmented Plane Wave Plus Local Orbitals Program for Calculating Crystal Properties* (Technical Universität, Wien, Austria, 2012).
- [58] G. N. Darriba, R. Faccio, and M. Rentería, *Physica B (Amsterdam, Neth.)* **407**, 3093 (2012).
- [59] L. A. Errico and M. Rentería, *Phys. Rev. B* **73**, 115125 (2006).
- [60] L. Errico, K. Lejaeghere, J. Runco, S. N. Mishra, M. Rentería, and S. Cottenier, *J. Phys. Chem. C* **120**, 23111 (2016).